CrossMark
click for updates

Nanoparticle characterization based on STM and STS

Shinya Kano,†[a] Tsukasa Tada[a] and Yutaka Majima*[ab]

In this review, we describe recent progress made in the study of nanoparticles characterized by scanning tunneling microscopy (STM) and scanning tunneling spectroscopy (STS). Basic principles of STM measurements and single-electron tunneling phenomena through a single NP are summarized. We highlight the results of electrical and photonic properties on NPs studied by STM and STS. Because nanoparticles are single-digit nanometre in diameter, a single-electron transport on individual nanoparticles such as Coulomb blockade and resonant tunneling through discrete energy levels are investigated. Photon-emission from NPs is also introduced based on STM measurements. Novel single-nanoparticle functions such as stochastic blinking and one-write erasing behaviours are presented. This review provides an overview of nanoparticle characterization methods based on STM and STS that include the detailed understanding of the electrical and photonics properties of nanoparticles.

1 Introduction

Scanning tunneling microscopy (STM) is an indispensable technique in the current research fields of nanoelectronics and surface science.[1–7,9–11] STM was developed by researchers

[a] *Materials and Structures Laboratory, Tokyo Institute of Technology, Yokohama 226-8503, Japan. E-mail: majima@msl.titech.ac.jp*

[b] *Department of Printed Electronics Engineering, Sunchon National University, Sunchon 540-742, Republic of Korea*

† Present address: Department of Electrical and Electronic Engineering, Graduate School of Engineering, Kobe University, Kobe 657-8501, Japan.

Binnig and Rohrer, at the IBM Zurich Research Laboratory in 1982 to observe the (110) surfaces of $CaIrSn_4$ and Au.[1] STM has revealed many intriguing surface structures such as the 7×7 reconstruction of a Si(111) surface[6] and highly oriented pyrolytic graphite (HOPG).[7] Gaining atomic resolution in STM is a major motivation in surface science as the technique would allow researchers to obtain images of individual atoms and molecules in real space. Because of the molecular resolution, STM can display local electrical characteristics of nanomaterials by scanning tunneling spectroscopy (STS). The conductivity of a single nanomaterial particle such as carbon

Shinya Kano received his PhD degree from the Department of Materials Science and Engineering from Tokyo Institute of Technology (Tokyo Tech) in 2013. He was a visiting researcher in the Cavendish Laboratory, University of Cambridge, UK, in 2013. He has been an Assistant Professor in the Department of Electrical and Electronic Engineering, Kobe University, since 2014. His current research is on the application of functional nanomaterials to nanodevices.

Shinya Kano

Tsukasa Tada received the BS, MS, and PhD degrees in quantum chemistry from Kyoto University in 1973, 1975, and 1987, respectively. After joining the Toshiba R & D Center in 1975, he was with the VLSI Cooperative Laboratories from 1976 to 1980. Besides his research and development work in electron resist materials for VLSI, he has carried out quantum chemical studies on electronic materials, Si LSI device processing technology, and molecular devices

Tsukasa Tada

at Toshiba R & D Center. He has been a research member of Tokyo Institute of Technology since 2014. Dr Tada is a member of the Chemical Society of Japan, the American Chemical Society, and the Japan Society of Applied Physics.

nanomaterials[8,12–15] and organic molecules[16–22] has been determined by STS.

Colloidal synthesized nanoparticles (NPs) are interesting nanomaterials for future nanoelectronics and bioelectronics applications because of their unique electronic and opto-electronic properties.[23–36] The electronic properties of NPs are strongly dependent on their size and ligand molecules. The size of NPs is typically in the nanometre scale, and determines the energy band.[37,38] In the synthesis of NPs, the diameter can be precisely controlled to the sub-nanometre scale.[39–50] Consequently, the bandgap of semiconductor NPs[36,51,52] and mean energy level spacing[53,54] can be tuned by the synthesis.[24] A variety of chemical properties can be designed by selecting and controlling the ligand molecules surrounding the NPs. This surface functionalization is widely used for enhancing the solubility in a solvent or imparting chemical reactivity to the metallic surface.[32,40,55] The synthesis of NPs has been established and the mass production of size-controlled NPs can be achieved. These advantages lead to practical applications for synthesized NPs in solid-state electronic devices.

Several applications for NPs have been reported: single-electron transistors (SETs),[53,54,56–68] switches,[31,69] and light-emitting diodes.[31,70] To design nanodevices with NPs, it is necessary to evaluate the intrinsic properties of a single NP, such as the conductivity and quantum tunneling effect. STM and STS are the most suitable techniques to simultaneously obtain both a single-dot image and its electrical properties. Coulomb blockade phenomena[71–85] and single-NP switching[49,86,87] have been recently reported at room temperature ($T \approx 300$ K) as well as low temperatures ($T = 4.2$–100 K). Therefore, it is important to understand what information of the synthesized NPs can be obtained from the STM and STS measurements.

Here, we review recent progress in the characterization of NPs based on STM and STS for applications of nanodevices. In Section 2, the basic principles of STM and STS are summarized to understand their advantages for this investigation. In Section 3, several types of synthesized NPs are reviewed. We also discuss established techniques to deposit NPs on a conductive substrate for STM analysis. In Section 4, we highlight the results of electrical and photonic characterization of NPs by STM and STS. Recent literature describing methods for obtaining useful functions of NPs and their ligands is also summarized.

2 Experimental background

2.1 Scanning tunneling microscopy

The atomic-resolution of STM is attributed to the imaging mechanism based on the quantum tunneling phenomena. STM measures the tunneling current I that is generated by a bias voltage V between the atomically sharp STM tip and the material surface. The tunneling current increases by an order of the current for every 1 Å reduction in distance.[3,8] The distance in the xyz-directions is also controlled by a piezoelectric scanner, which provides angstrom-order changes in the distance, and a feedback loop, which controls the z-direction, is installed to keep the tunneling current constant. By observing the tunneling current as the tip scans a surface, the morphology of the surface can be precisely detected. Measurements can be carried out at room temperature in solution as well as at low temperature under ultra-high vacuum (UHV) conditions.[9] We can obtain various electrical properties of an object by analyzing the tunneling current, such as the local density of states (LDOS) from dI/dV and local barrier height from dI/dz.[3]

Fig. 1 shows a schematic view of scanning a metallofullerene and alkanethiol self-assembled monolayer (SAM) on an Au(111) surface by STM. Alkanethiol SAMs self-assemble on an Au(111) surface to form a $\sqrt{3} \times \sqrt{3}R30°$ structure.[15,88–91] Fig. 2 shows the STM image of a Lu endohedral metallofullerene (Lu@C$_{82}$) on an octanethiol SAM/Au(111) surface.[15] The octanethiol molecules form SAMs on the Au(111) surface at a distance of 0.50 nm. It is noted that the corrugated surface of the metallofullerene reflects the LDOS in the molecule. The reason why the LDOS affects the STM topography images will be explained later.

Yutaka Majima received BS, MS and Dr of Engineering degrees from the Department of Electrical and Electronic Engineering from Tokyo Institute of Technology (Tokyo Tech), Japan, in 1987, 1989 and 1992, respectively. In 1992, he joined Toshiba Corporation, and became a Research Scientist in 1996. In 1996, he moved to Tokyo Tech as an Assistant Professor. He became an Associate Professor of the Department of Physical Electronics, Tokyo Tech in 1998. He has been Professor of Materials and Structures Laboratory, Tokyo Tech since 2009. His research covers nanoscale electronic devices and scanning tunneling microscopy.
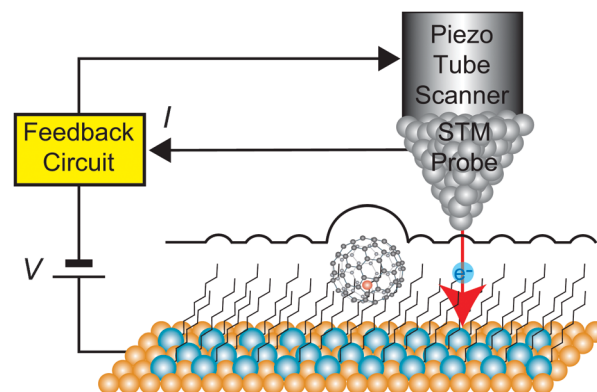
Yutaka Majima

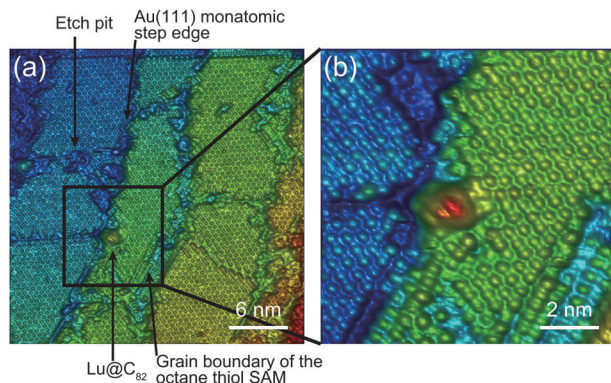Fig. 1   Schematic view of STM circuits in a constant-current mode.

Fig. 2 (a) and (b) Molecular-resolution 3D STM images of a Lu@C_{82} adsorbed on an octanethiol SAM/ an Au(111) surface at 65 K.[15] Reprinted with permission from M. Iwamoto, D. Ogawa, Y. Yasutake, Y. Azuma, H. Umemoto, K. Ohashi, N. Izumi, H. Shinohara and Y. Majima, *J. Phys. Chem. C*, 2010, **114**, 14704–14709. Copyright 2010 American Chemical Society.
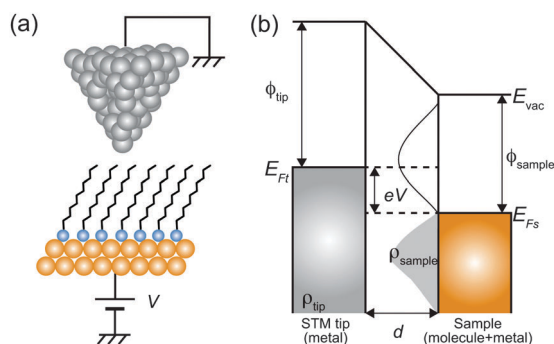

Fig. 3 (a) Schematic illustration of an STM tunneling junction consisting of an alkanethiol SAM on an Au(111) surface. (b) Schematic energy diagram of the STM tunneling junction. Here, E_{vac} is the vacuum energy level, E_{Ft} (E_{Fs}) is the Fermi energy of the tip (sample), ρ_{tip} (ρ_{sample}) is the density of states of the sample and the tip, ϕ_{tip} (ϕ_{sample}) is the work function of the tip (sample) metal, V is the applied sample bias voltage, and d is the distance from the sample to the tip.

Here, we describe the basic physical principles of STM measurements. Fig. 3(a) shows a typical STM tunneling junction comprising alkanethiol molecules on an Au(111) surface. To elucidate the basic principles of STM measurements as simply as possible, we have introduced an approximation that the electric potential of an alkanethiol monolayer is nearly identical to that of the metal electrode (Au).[92] By assuming this simple approximation, a schematic energy diagram of the STM junction can be illustrated as shown in Fig. 3(b).

In this simple model, when a bias voltage V is applied between the tip and the metal electrode, the transmission coefficient T' of the electrons through the potential barrier is approximated by the WKB approximation as[93]

$$T' \propto \exp\left[\frac{-2d}{\hbar}\sqrt{2m_e\left(\bar{\phi} + \frac{eV}{2} - E\right)}\right], \tag{1}$$

where d is the distance between the tip and the sample, m_e is the electron mass, E is the electron energy, $\bar{\phi} = (\phi_{tip} + \phi_{sample})/2$

is the average potential barrier height between the tip and the sample, $\hbar$ is the Dirac constant, and e is the elementary charge of an electron.

If a hard wall potential barrier (*i.e.* infinite potential barrier $\bar{\phi} = \infty$) exists in the direction of the wave, the electron is completely reflected by the wall ($T' = 0$). However, if a finite potential barrier exists ($\bar{\phi} \neq \infty$), there is some probability that the electron goes through the potential barrier even though the electron does not have enough energy to overcome the barrier ($T' \neq 0$).

The tunneling current can be obtained by the integration of the electron density ρ and the transmission coefficient T',[11]

$$I \propto \int_0^{eV} \rho_{tip}(E - eV)\rho_{sample}(E)T'(E, eV, d)dE, \tag{2}$$

where $\rho_{sample}(E)$ and $\rho_{tip}(E)$ are the density of states for the sample and the tip, respectively, at an electron energy E from the Fermi energy of the sample E_{Fs}, V is the bias voltage (defined as the sample bias with respect to the tip), and $T'(E, eV, d)$ is the tunneling transmission probability for electrons with energy E and applied voltage V over the distance from the sample to the tip d. This relationship indicates that the tunneling current between two metallic surfaces is determined by the distance and local density of states of the substrate. Therefore, STM images of a single molecule or a substrate itself reflect both their LDOSs and height information.[13,15,22,94–98]

By considering the tunneling-distance dependence, the transconductance G of the material can be represented as follows,

$$G \propto A \exp(-\alpha z), \tag{3}$$

where α is the decay constant of the material, z is the tip–sample separation, and A is a constant value. This equation leads to the tunneling current changing by an order of magnitude when the value of z changes by 1 Å (Fig. 4). Measuring dI/dz indicates the conductivity of the observed nanomaterial, for example, $\alpha = 2.3$ Å^{-1} in a vacuum or $\alpha = 1.1$ Å^{-1} in alkanethiol molecules.[8,16,18,20]

The conductance of a single nanomaterial particle can be measured using STM by two methods. One is a break junction technique, which measures the conductance between the tip
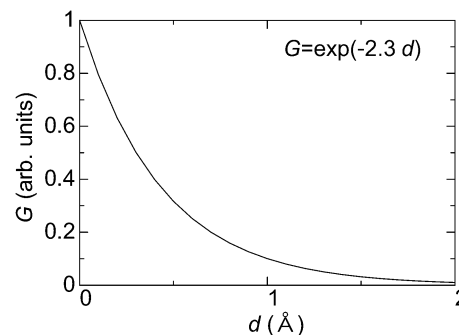

Fig. 4 Typical relationship between transconductance (G) and thickness of materials (d) in a vacuum.

and the substrate while raising the tip.[19,99–101] The peak conductance in the statistical histogram represents the conductance of a single molecule.

The other method is the STS technique for directly measuring the current–voltage (I–V) characteristics of a single molecule. In the investigation of a single NP, STS is usually adopted because single-electron tunneling phenomena can be simultaneously characterized in the current as a function of voltage. Therefore, we only consider the STS technique in further sections of this review.

2.2 Scanning tunneling spectroscopy

STS can achieve electrical characterization of a local point on a nanomaterial by monitoring the I–V characteristics. An STM tip is positioned over a sample keeping the feedback loop off during the measurements; therefore, the STS measurements can obtain the electrical characteristics of a truly single molecule or NP.

If the tunneling current through the sample is represented by eqn (2), the value of dI/dV is given as follows,

$$\frac{dI}{dV} \propto e\rho_{sample}(eV)\rho_{tip}(0)T'(eV,eV,d), \quad (4)$$

assuming that d is constant during the measurements. Therefore, the differential conductance dI/dV is proportional to the LDOS of the sample ρ_{sample} if the applied voltage is low and $\rho_{tip}(0)$ is constant.[1,4,5,11] For NPs, the LDOS corresponds to the discrete zero-dimensional (0D) energy spectrum or energy bandgap. Spatial mapping of dI/dV in the STM image can be achieved by current-imaging tunneling spectroscopy (CITS). CITS is useful for investigating the spatial distribution of the LDOS over an entire molecule.[15,22,82,102]

Electron tunneling is treated as an elastic process in the above discussion; however, a small amount of current is also provided by inelastic tunneling processes of electrons through the tunneling barrier. Vibrational modes of organic molecules can be detected by measuring dI^2/dV^2 characteristics using a lock-in amplifier, which is called inelastic tunneling spectroscopy (IETS).[103–105] In IETS measurements, electrons release an energy of $\hbar\omega$ through the inelastic tunneling process as phonon vibrations ω of the nanomaterials. STM is also useful in nanophotonics to observe locally excited luminescence and plasmonic modes in nanostructures, as well as electrical characterization.[106–108] In this case, the energy released from the tunneling electrons is converted into photonic energy, which excites photons from the nanomaterial. The simultaneous observation of topographies and photon-emission maps is realized by the combination of STM and an avalanche photodiode to count the number of photons.[108] However, we can exclude the effects of inelastic tunneling processes in the STS measurements as long as the contribution of the inelastic tunneling process is small. Therefore, we keep two viewpoints in mind to analyze the STS characteristics: direct tunneling and single-electron tunneling.

2.2.1 Direct tunneling. When a single tunneling barrier, such as a vacuum or an organic molecule, insulates the STM tip from the metallic substrate, tunneling current flows between
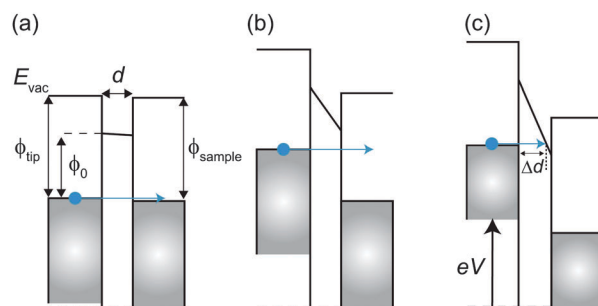

Fig. 5 Schematic energy band diagram of three types of tunneling behaviors in metal/insulator/metal structures: (a) $eV \simeq 0$, (b) $eV > \bar{\phi}$ and (c) $eV > \bar{\phi}$. ϕ_0 is the barrier height of the insulator $\bar{\phi}$ is the average barrier height of the insulator. Δd is the tunneling distance of an electron and d is the thickness of the insulator.

them (Fig. 3(a)). Simmons summarized three types of tunneling behaviors in the analysis of electrical characteristics: (a) $eV \simeq 0$, (b) $eV < \bar{\phi}$, and (c) $eV > \bar{\phi}$, where the average barrier height of the insulator was $\bar{\phi}$.[93] The three types of tunneling behaviors are shown in Fig. 5. When the temperature $T = 0$, the tunneling current density J can be written as

$$J = J_0[\bar{\phi}\exp(-A\bar{\phi}^{\frac{1}{2}}) - (\bar{\phi} + eV)\exp[-A(\bar{\phi} + eV)^{\frac{1}{2}}]], \quad (5)$$

where $A = 4\pi\beta\Delta d\sqrt{2m_e}/h$, $J_0 = e/(2\pi h\Delta d^2\beta^2)$, h is the Planck constant, Δd is the tunneling distance through an insulator, and β is a correction factor.

Characterization based on this basic analysis has been carried out to understand the electrical properties of organic molecules and nanogap electrodes.[18,109–111] To understand the electrical behaviors, tunneling phenomena at the several-nanometre scale must be considered.

2.2.2 Single-electron tunneling. If double-barrier tunneling junctions (DBTJ) comprising a single conductive island between two metallic electrodes are formed between the STM tip and the substrate, single-electron tunneling appears through the barriers. The single conductive island in a DBTJ is called a Coulomb island. Several nanomaterials on a metallic substrate, such as organic molecules and NPs, can behave as Coulomb islands. Fig. 7(a) shows a schematic diagram of a DBTJ comprising a decanethiol-protected Au NP anchored by a decanedithiol molecule on an Au(111) surface.

Typical experimental I–V characteristics of the DBTJ consisting of an STM tip/vacuum/octanethiol ligand/Au core/decanedithiol anchor molecule/Au(111) substrate are shown in Fig. 6 (solid line), which was measured by STS. A clear Coulomb staircase including Coulomb gap and first and second stairs for positive and negative bias voltages has been observed.

An equivalent circuit diagram of this DBTJ is shown in Fig. 7(b). Tunneling junction 1 (2) is expressed as a parallel of tunneling resistances R_1 (R_2) and capacitances C_1 (C_2), respectively. Here, we consider that junction 1 consists of a vacuum and ligand molecules, and junction 2 consists of only a decanedithiol.

Single-electron tunneling can be described by the orthodox theory.[81,112–114] A single electron can tunnel into the island when electrostatic conditions are present for the entire circuit;
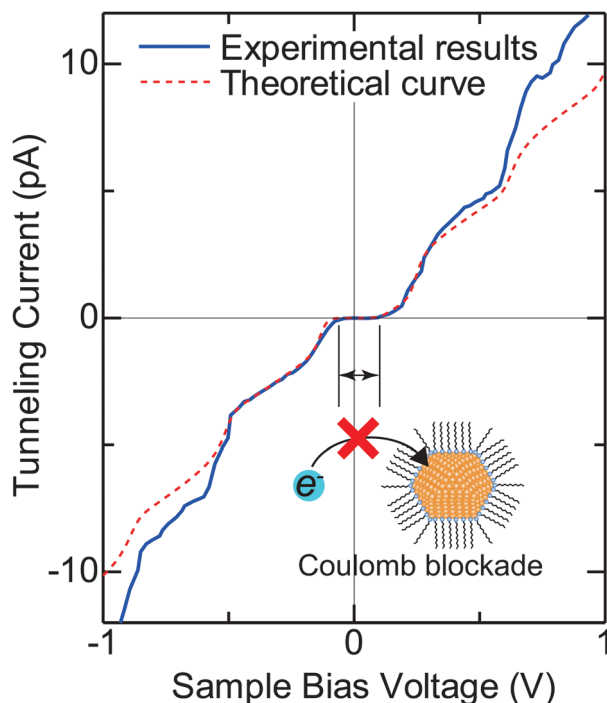
This journal is © The Royal Society of Chemistry 2015

Chem. Soc. Rev., 2015, 44, 970–987 | 973

Fig. 6 Typical experimental I–V characteristic of the DBTJ consisting of an STM tip/vacuum/octanethiol ligand/Au core/decanedithiol anchor molecule/Au(111) substrate (solid line). An experimental Coulomb staircase is clearly observed. The dashed line represents the theoretical curve calculated by the orthodox theory. The inset is the schematic of the Coulomb blockade effect that is observed near $V = 0$.

the total energy after changing the number of electrons in the island is smaller than the energy of the initial states. The change in the total energy when an electron tunnels through junction 1 $\Delta E_1^\pm$ is given by

$$\Delta E_1^\pm(n) = \frac{e^2}{2C_\Sigma} \pm \frac{e}{C_\Sigma}(ne + Q_0 \mp C_2 V), \qquad (6)$$

and for tunneling through junction 2, $\Delta E_2^\pm$ is given by

$$\Delta E_2^\pm(n) = \frac{e^2}{2C_\Sigma} \pm \frac{e}{C_\Sigma}(ne + Q_0 \pm C_1 V), \qquad (7)$$

where n is the number of electrons in the Coulomb island, $C_\Sigma = C_1 + C_2$ is the total capacitance of the DBTJ, and Q_0 is the fractional residual charge surrounding the island. When $\Delta E_1^\pm$ and $\Delta E_2^\pm$ are larger than zero, single-electron tunneling is suppressed because the electrostatic energy after electron tunneling becomes larger than that of the initial states. This suppression is called a Coulomb blockade (Fig. 7(c)). Electrons can tunnel through the junction one by one only if $\Delta E^\pm$ for the junction becomes negative (Fig. 7(d)).

To observe the Coulomb blockade clearly, it is necessary to satisfy the energy-scale condition:

$$k_B T < \frac{\hbar}{RC_\Sigma} < E_c, \qquad (8)$$

where k_B is the Boltzmann constant, T is the temperature, R is the resistance of the tunneling junction, and $E_c = e^2/2C_\Sigma$ is the
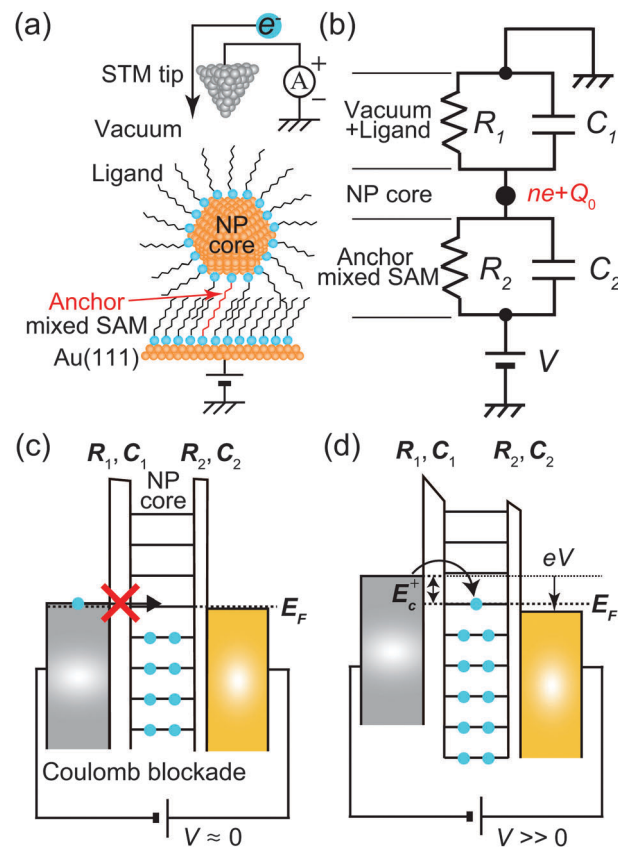

Fig. 7 (a) Schematic image of DBTJs consisting of a single octanethiol protected Au nanoparticle on the Au(111) surface. (b) Equivalent circuits of the DBTJs. (c) and (d) Schematic energy band diagrams of DBTJs. (c) Coulomb blockade conditions. Electron tunneling is prohibited. (d) Allowed tunneling conditions because of sufficient energy (E_c^+) given by voltage.

charging energy. This condition limits the observation temperature of the Coulomb blockade.

The tunneling resistance of R_1 can be adjusted by a tunneling current through a DBTJ (set-point current). In contrast, the resistance of R_2 is expected to be constant owing to the ligand molecules. The overall shape of the Coulomb staircase strongly depends on the tunneling resistance ratio R_1/R_2 as shown in Fig. 8; therefore, we can estimate the values of the tunneling resistance in the junctions.[72,81,84,87] In evaporated Au NPs on dodecanethiol/Au(111) surfaces, it was reported that the total resistances ($R_1 + R_2$) and the total capacitances ($C_1 + C_2$) of DBTJs can be controlled by changing the set-point current in the STM system.[72] The tunneling resistances in the DBTJs can be estimated as a unique value if $1 < R_1/R_2 < 50$ when R_1 is larger than R_2.[81] Under these conditions, we can estimate the resistance R_2 between a NP and an Au(111) surface, which corresponds to the resistance of the linker molecules, by fitting the I–V curves with the orthodox theory.

One interesting application of a Coulomb blockade is a single-electron transistor, which comprises a DBTJ and gate electrodes capacitively coupled to a Coulomb island.[115] Single-electron transistors can be used as single-electron memory,[116] a single-electron pump,[117] and multiple logic circuits.[63]

974 | Chem. Soc. Rev., 2015, **44**, 970–987
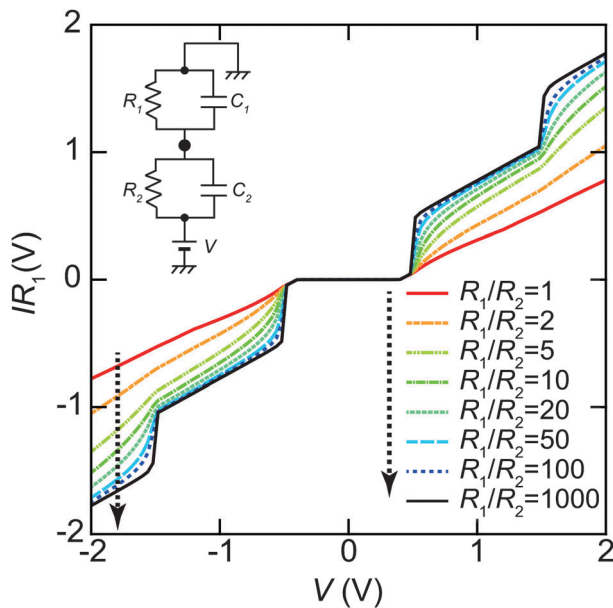
This journal is © The Royal Society of Chemistry 2015

Fig. 8 Set-point current dependence of the whole shape of Coulomb staircases. These curves are simulated by the orthodox theory[81,114] using R_1/R_2 = 1, 2, 5, 10, 20, 50, 100 and 1000, respectively (indicated by the dashed arrow in this order). The circuit parameters are R_1 = 0.1–100 GΩ, R_2 = 0.1 GΩ, C_1 = 0.16 aF, C_2 = 0.20 aF, Q_0 = 0e and T = 4.2 K. The vertical axis is normalized by multiplying R_1 to compare the whole shape of the Coulomb staircase. A higher R_1/R_2 value gives a sharper Coulomb stair-case; in contrast, the shapes of the curves are not dependent on R_1/R_2 values under R_1/R_2 > 50.

Fig. 9 (a) Theoretical capacitances C_{dot} of a free sphere (solid lines), between a single conductive sphere and a conducting plate (dashed lines). (b) Corresponding charging energy E_c = $e^2/2C_{dot}$ of a free sphere (solid lines), between a single conductive sphere and a conducting plate (dashed lines). The value of a relative dielectric constant ε_r in alkanethiol (2.6) is used above calculations. (c) Simulated E_c/k_BT dependence of Coulomb staircases. The values of E_c/k_BT are 1, 2, 5, 10, 20, 50 and 100 in the order as indicated by the dashed arrow. The circuit parameters are, R_1 = 1 GΩ, R_2 = 0.1 GΩ, C_1 = 6.0 aF, C_2 = 6.0 aF, Q_0 = 0e and E_c = 6.7 meV (comparable to a thermal energy at 77 K). (d) Calculated mean energy level spacing ΔE of Au NP and Si NC (nanocrystal). Here, R represents a diameter of NPs.

Room-temperature single-electron transistors have been reported using metallic NPs,[58,59] Si NPs,[118–121] and carbon nanotubes.[122,123] The charging energy of a single-electron transistor is an important parameter to determine the operating temperature following eqn (8). We can evaluate the charging energy of a single NP by the STS measurement and the orthodox theory. Thus, STM and STS are useful tools to explore candidates for Coulomb islands in single-electron transistors.

2.3 Charging energy of nanoparticles

Here, we evaluate the charging energy of NPs to show that synthesized NPs are promising for practical applications of quantum effects. Fig. 9(a) shows the theoretical capacitance between a single conductive sphere and a conducting plate, which is proportional to the capacitance of a sphere in free space.[124,125] The corresponding charging energy is estimated in Fig. 9(b). The charging energy increases as the size of the Coulomb island decreases. The simulated E_c/k_BT dependence of the Coulomb staircase is shown in Fig. 9(c). The I–V curves are calculated by the orthodox theory and it is clear that this simulation follows eqn (8). Moreover, this simulation indicates that E_c is required to be much larger than a thermal fluctuation to observe a clear zero conductance region. The zero conductance region of the Coulomb blockade is critical to maintain the on/off ratio in a single-electron transistor. Therefore, Coulomb islands less than 2 nm in diameter are desired for
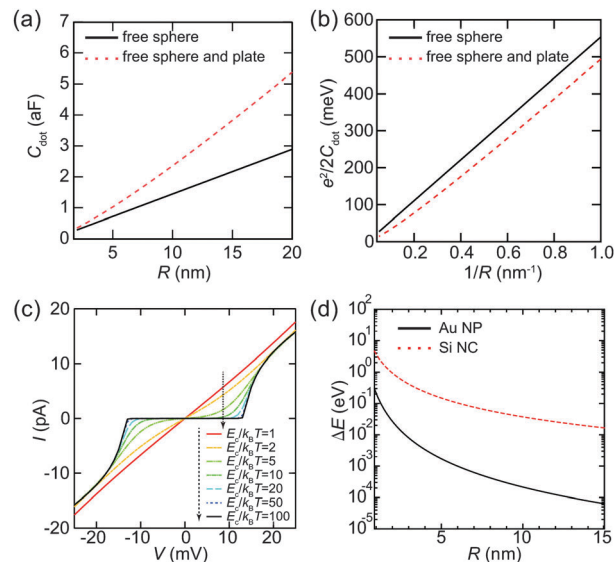
room-temperature operation, e.g., E_c > 260 meV where E_c is 10 times larger than the thermal energy at 300 K.

When the diameter of NPs is lower than 2 nm, we need to consider the effect of the discrete 0D energy levels caused by quantum confinement, even at room temperature. Fig. 9(d) shows an example of the discrete energy level spacing ΔE in Au NPs and Si nanoclusters (NCs). The value of ΔE in the metallic Au NPs is directly derived from the density of states at the Fermi energy and volume $\Delta E \approx 2\pi^2\hbar^2/(m_{Au}k_FV)$, where m_{Au} is the electron mass in Au (1.1 m_e) and k_F is the Fermi wavenumber in Au.[23,126] This assumption is valid when the Fermi level is in a half-filled band (i.e., metallic NPs), which implies that a number of electrons exist in the NPs. Therefore, the 0D levels are randomly dispersed along the energy axis, and the value of ΔE in metallic NPs describes a mean spacing between the levels.

In contrast, the value of ΔE in semiconductor NPs is estimated by the potential well of a quantum sphere $\Delta E \approx \pi^2\hbar^2/(2m_{Si}(R/2)^2)$, where m_{Si} is the electron mass in Si (0.40 m_e).[127,128] This corresponds to an energy difference between the ground state and the first excited state of the classical quantum sphere model. Semiconductor NPs have a few electrons because the Fermi level is in its bandgap; thus, the 0D levels tend to follow the electron-shell filling described by the potential-well approximation. This simple 0D-level spectrum is attributed to the observation of a predictable atomic-shell filling in semiconductor NPs (shown later).

This journal is © The Royal Society of Chemistry 2015

Chem. Soc. Rev., 2015, 44, 970–987 | 975

Semiconductor NPs generally have larger energy spacings than metallic NPs of the same diameter.[129] The condition to observe the effect of discrete energy levels is $\Delta E > 3.5k_BT$, which was derived from the thermal broadening of Fermi–Dirac distributions in metallic lead electrodes.[130]

To harness these quantum effects practically, it is critical to control the size of the Coulomb islands. Electron configurations of elemental atoms are precisely determined by the number of atomic nuclei. Coulomb islands of a single-donor atom in Si have been reported as single-atom transistors, which show a charging energy or resonant spectrum in accordance with the excited state of the single donor.[131–133] These results indicate that precisely size-controlled Coulomb islands show reproducible quantum effects. Synthesized NPs have several advantages: size control in the sub-nanometre scale, ability for mass production, and reproducibility. Thus, synthesized NPs are promising materials to exhibit the above-mentioned quantum effects.

3 Synthesized nanoparticles

For stable metallic NPs, noble metals such as Au, Ag, and Pt are used because they are not easily oxidized.[31] Synthesized NPs are usually surrounded by ligand molecules to prevent aggregation.

One of the most famous techniques to synthesize metallic NPs is the Brust–Schiffrin method for Au NPs.[40,43] Temperature- and air-stable, size-controlled Au NPs can be mass produced by this method and can be functionalized by ligand molecules.[27,134–136] Teranishi *et al.* controlled the core diameter of decanethiol-protected Au NPs from 3.4 ± 0.3 nm to 6.8 ± 0.5 nm by revealing the appropriate heat-treatment temperatures during synthesis.[45] The number of Pt atoms (13, 55, 147, 309, *etc.*)[137,138] and Au atoms (10, 15, 18, 22, 25, *etc.*)[48] occurs in the well-known magic numbers. As the magic number is determined by the crystalline structure of the NPs, the size of the nanoparticles can be identical. Therefore, if we utilize the magic number of atoms in single-electron devices, the charging energy of the Coulomb islands and the 0D-level spacing can be identical.

Several thiol-derivatized molecules are used as ligands, the same as alkanethiol molecules, such as amino-type molecules,[46] glutathione thiolate,[47,48] porphyrin,[49] and oligo(phenylene-ethynylene) (OPE) molecules.[50] The synthesized NPs can be stored in the solid state under ambient conditions and redissolved in common organic solvents. Semiconductor NPs can also be synthesized by established methods to fine-tune the diameter in the sub-nanometre scale.[51,52,55,139–142] Because of these advantages, synthesized NPs are intensively used in the field of nanoelectronics. Reported synthesized NPs are summarized in Table 1.

Table 1 Several types of synthesized NPs. The ligand and the core diameter (R) of the NPs are summarized

Elements	Ligands	R (nm)	Ref.
Au	$CH_3(CH_2)_9SH$	2.0–2.5 ± 1.0	40
Pt	Phenanthroline, O_2	1.5–2.5	39, 137, 177
Au	Phosphine, Cl	1.4	39
Pd	Poly(N-vinyl-2-pyrrolidone)	2.2 ± 0.4	143
Au	$CH_3(CH_2)_{11}SH$	3.4 ± 0.3	45
Au	$CH_3(CH_2)_5SH$, $HS(CH_2)_6SH$	2.2	42
Au	$CH_3(CH_2)_{11}SH$	2.1 ± 0.3	144
Ag	$CH_3(CH_2)_{11}SH$	5.5 ± 0.3	144
Pd	$CH_3(CH_2)_{11}SH$	6.3 ± 0.4	144
Au/Ag alloy	$CH_3(CH_2)_{11}SH$	3.8 ± 0.2	144
Co	$CH_3(CH_2)_{11}COOH$	5.5 ± 1.0	194
Au	$CH_3(CH_2)_{17}SH$	0.8 ± 0.2	44
	N,N-dimethylaminoethanethiol		
	Mercaptoethanesulfonic acid		
Au or Ag	$CH_3(CH_2)_7SH$ and $HOOCCH_3(CH_2)_2SH$	3.7	217
Au	C_{60}	2	136
Pd	Polyvinylpyrrolidone	2.5	185
Au	Polyvinylpyrrolidone	1.7	185
Au	Amino-type molecule	2.4 ± 0.2	46
Au	Glutathione	0.7	48
Au	Thiol-derivatized OPE	1.7 ± 0.3	49
Au	Thiol-derivatized porphyrin	1.1 ± 0.2	50
CdS, CdSe, CdTe	Trioctylphosphine	3.7 ± 0.2	139
	Trioctylphosphine oxide		
InP	Trioctylphosphine	2.6–4.6	142
	Trioctylphosphine oxide		
GaP	Trioctylphosphine	3.0	142
	Trioctylphosphine oxide		
InAs	Trioctylphosphine	2.5–6.0 ± 10%	141
CdS	N/A	2.1 ± 0.3%	165
CdSe	Trioctylphosphine oxide	5 ± 0.5	201
	Hexadecylamine		
PbSe	Oleic acid	3 ± 0.3	201

N/A: not mentioned in the paper.

The deposition of synthesized NPs is important in the practical application of NPs; such deposition is classified into two types of absorption: physisorption and chemisorption. Dropcast, spincoat, and Langmuir–Blodgett methods are widely used as physisorption processes to form monolayers of NPs on flat substrates. The interacting force between the NPs and the substrates is mainly caused by only van der Waals interactions. Conversely, chemisorption processes are based on chemical reactions between the NPs and the functionalized substrates with SAMs. The interacting forces in chemical interactions are stronger than van der Waals forces, which make the NPs stable on the substrates.

Controlling the density of NPs by the density of tether molecules on the substrate is a notable advantage in the chemisorption process. Alkanethiol–alkanedithiol-mixed SAMs can be formed by immersing Au(111) substrates into alkanethiol and alkanedithiol solutions successively.[145–147] The inserted alkanedithiols in alkanethiol monolayers can be observed by STM or atomic force microscopy (AFM).[83,145–147] In ref. 83, the density of chemisorbed Au nanoparticles was controlled in $1/100 \times 100$ nm^2 in 0.5 mM octanedithiol solution and $39/100 \times 100$ nm^2 in 50 mM solution. Electrically stable SETs (chemically assembled SETs) have been demonstrated by using the same chemisorption process to deposit a single synthesized Au NP between size-regulated nanogap electrodes formed by electroless-gold plating.[54,60–65] Therefore, chemisorption is more promising than physisorption for stable and ideal electrical transport through the NPs by STM and STS.

In this section, we explained the advantages of the synthesized NPs. Chemical assembly processes are more suitable for stable chemisorption of NPs on a substrate.

4 Single-nanoparticle properties by scanning tunneling microscopy

4.1 Single-electron transport of single nanoparticles

In the early stages, single-electron transport in metallic NPs was mainly investigated by using STM. The NPs for STM investigation were made by thermal evaporation. Because metals naturally tend to nucleate into particles, a small amount of evaporation (less than 1 nm) can generate hemispherical NPs for small metal droplets on a thin insulator.[148–150] In the first report of single-electron transport in NPs, a Coulomb staircase was observed at 4.2 K in a structure comprising a granular layer of evaporated Au NPs in the oxide layer between two Ag or Cu films.[151] Because multiple current paths exist as parallel arrays of junctions when this technique is used, the observed Coulomb staircase strongly depends on the variation in size or the number of NPs. Therefore, it is necessary to observe single-electron transport in a single NP by using STM and STS measurements.

A Coulomb staircase was first observed by STM in a structure comprising a granular Al layer on oxidized Al films.[152] The measurement temperature was 1.2 K and STS was carried out on a single granular Al dot. The observed Coulomb staircase had a periodic structure, which was explained by Monte Carlo simulations based on the DBTJ of a single Coulomb island.

This analysis proved that the single NP acted as a Coulomb island in this measurement. After this report, several evaporated NPs were investigated by STM and STS at low temperature, e.g., Al,[153] Au,[114,154,155] Co,[156] In,[157,158] Pt,[159,160] Pd,[161,162] and Si.[79]

To increase the observation temperature of the Coulomb blockade, it is necessary to form smaller NPs for Coulomb islands. To observe the Coulomb blockade at room temperature ($T = 300$ K), the charging energy needs to be much larger than the thermal fluctuation $k_B T$ (25.8 meV). We have shown in Fig. 9(c) that a much larger charging energy is required to observe single-electron transport without any random tunneling events. Therefore, the size of the NPs has to be on the order of 1 nm to observe the Coulomb blockade at room temperature.

Schönenberger et al. reported a Coulomb staircase on Au-evaporated NPs/ZrO$_2$ (1 nm)/Au film at room temperature in air.[71] The schematic image of the structure and STS characteristics are shown in Fig. 10(a) and (b), respectively. To increase the charging energy, the ideal height and diameter of the NPs were 0.2 nm and 4 ± 0.5 nm, respectively. The charging energy of the DBTJ was 70 meV, which is larger than 26 meV at 300 K; therefore, a room-temperature Coulomb staircase was observed.

Next, organic SAMs were introduced as tunneling barriers. Initially, the tunneling barrier between the NPs and the substrate was the oxidized layer. Because the tunneling current strongly depends on the distance, the thickness of the insulating layer
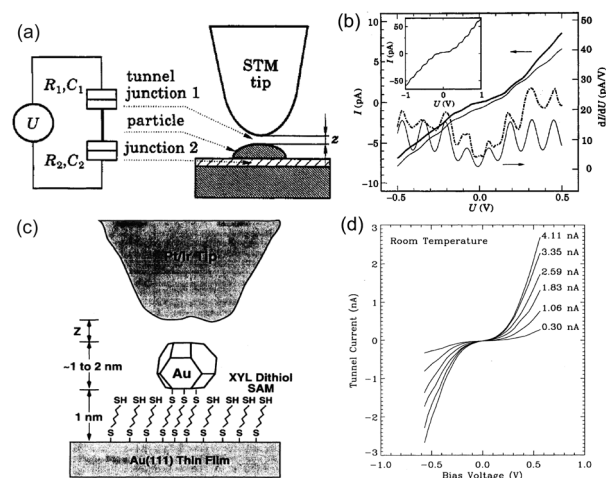

Fig. 10 (a) Right: schematic image of the STM tip above an evaporated Au NP/ZrO$_2$ (1 nm)/Au structure. The Au NP was physically adsorbed on the ZrO$_2$ layer. Left: equivalent circuit of DBTJs. (b) Coulomb staircase at room temperature. Thick solid and dash-dotted curves represent I–V characteristics and the numerical differential conductance. Thin solid curves are obtained from theory and shifted vertically for clarity. Inset: Coulomb staircase at 4.2 K.[71] Reprinted with permission from C. Schönenberger, H. Van Houten and H. C. Donkersloot, Single-Electron Tunnelling Observed at Room Temperature by Scanning-Tunnelling Microscopy. Eur. Phys. Lett., 1992, **3**, 249–254. http://iopscience.iop.org/0295-5075/20/3/010. (c) Schematic image of an evaporated Au NP/dithiol SAM/Au(111) substrate. The Au NP was chemically anchored by the dithiol molecules. (d) Coulomb blockade at room temperature on a tethered 1.8 nm Au NP.[73] Reprinted figures with permission from M. Dorogi, J. Gomez, R. Osifchin, R. P. Andres and R. Reifenberger, Phys. Rev. B: Condens. Matter Mater. Phys., 1995, **52**, 9071–9077. Copyright 1995 by the American Physical Society.

This journal is © The Royal Society of Chemistry 2015

Chem. Soc. Rev., 2015, **44**, 970–987 | 977

has to be atomically controlled. When a SAM acts as the tunneling barrier, we can control the thickness of the tunneling barrier by the length of the molecules. Alkanethiol molecules are the most famous SAMs, which consist of an alkyl chain with a thiol end group. Alkanethiol works as an insulator because all covalent chemical bonds are localized between the atoms (*i.e.*, σ-bond). The length of an alkanethiol molecule increases by 0.13 nm with each addition of a carbon atom in the alkyl chain.[163] Thus, an alkanethiol on the structure of the metal NP/alkanethiol/metallic surface is expected to help control the thickness of the tunneling barrier between the metals on the order of an angstrom.

In 1994, a room-temperature Coulomb staircase was demonstrated by STS for deposited Au NPs/alkanethiol/Au(111) film.[72] The diameter and height of the Au NPs were 5–10 and 2–3 nm, respectively. The charging energy was estimated to be 180 meV by a rough capacitance evaluation using parallel-plate capacitor models. In later reports, double-ended thiol molecules (alkanedithiol) were also used as linkers between the deposited NPs and the Au(111) surfaces for the chemisorption of NPs. To realize more stable Coulomb staircases at room temperature, α,α′-xylyldithiol and 4,4′-biphenyldithiol SAMs were used to bind NPs deposited on an Au(111) surface by a cluster beam (Fig. 10(c) and (d)).[73–75] A multiple expansion cluster source can generate Au NPs on the SAMs with diameters of ≈ 2 nm and heights of ≈ 1 nm. The resistance between a single Au NP and an Au(111) surface was estimated to be 18 ± 12 MΩ. This value corresponds to the calculated resistance of 4.5 ± 0.50 MΩ by the Landauer formula $R' = (h/2e^2)T'$.[164] Deposited CdS,[165,166] Co,[167] and Pt NPs[168,169] on SAMs were also studied. Recently, 0D levels of evaporated Au NPs on a 1,4-benzenedimethanethiol/Au(111) substrate were confirmed at 78 K.[170]

The coverage of Au deposited on octanethiol/Au(111) was investigated to determine the morphology of growing Au NPs.[171] The self-capacitance of a single deposited Au NP on octanedithiol/Au(111) was strongly dependent on the surface coverage and its diameter.[172–176] Sakotsubo *et al.* reported that the density of evaporated clusters can be controlled by using thiol–dithiol-mixed SAMs.[176] Their results suggest that an isolated Au NP is appropriate for investigating the Coulomb blockade behavior at room temperature because the surrounding Au NPs display a parasitic capacitance and decrease the charging energy.

Synthesized NPs are generally passivated by organic molecules to avoid aggregating and sintering, *i.e.*, they are initially covered by a tunneling barrier. The density of NPs deposited on a substrate can be controlled by changing the concentration of the NPs in solution, which is easier than controlling the density by evaporation methods. Because the NPs were isolated and size-controlled, synthesized NPs covered with ligand molecules were promising materials for Coulomb islands.

Initially, ligand-stabilized Pt NPs (comprising 309 Pt atoms) showed clear Coulomb staircases in STS measurements at 4.2 K.[137,177] Several years later, the Coulomb staircases for a single synthesized Au NP with an atomic mass unit (amu) of 29 k were reported at up to room temperature.[178,179] The Au NPs consisted of 147 ± 10 Au atoms in the core, corresponding to a diameter of 1.68 ± 0.04 nm, which was measured by mass
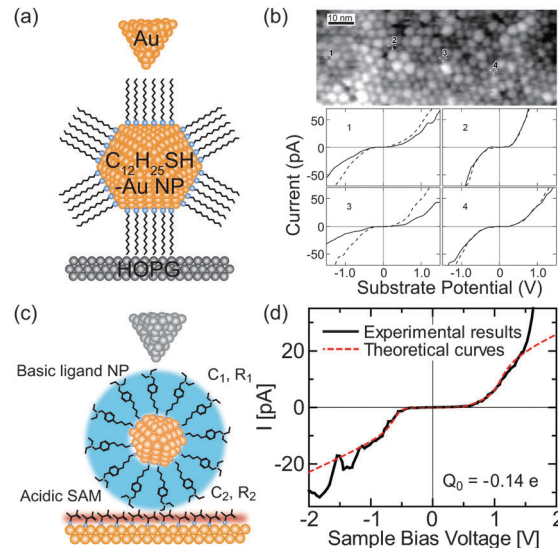

Fig. 11 Room-temperature Coulomb blockade on synthesized nanoparticles. (a) Schematic image of DBTJs consisting of Au-tip/dodecanethiol-protected Au nanoparticle/HOPG structures. (b) Room temperature Coulomb blockade at several NPs in the STM images.[179] Reprinted with permission from T. P. Bigioni, L. E. Harrell, W. G. Cullen, D. K. Guthrie, R. L. Whetten and P. N. First, *Eur. Phys. J. D*, 1999, **6**, 355–364. Copyright 1999 Springer-Verlag. (c) Schematic image of DBTJs consisting of PtIr-tip/bis-4,40-(4,4′-dithiobutylbenzyl)-*N*,*N*,*N*′,*N*′-tetraethylamine (TBA) protected Au NP/Au(111) structures. (d) Room-temperature Coulomb blockade on TBA protected Au NP with a 1.8 nm diameter.[84] Copyright (2011) The Japan Society of Applied Physics.

spectrometry.[179] The charging energy of the DBTJ was 75 meV, which was larger than the thermal fluctuations at room temperature (Fig. 11(a) and (b)).

Electrochemical cyclic voltammetry of Au-NPs solutions was used in an attempt to confirm the values of E_c by STS.[41,178,180] Current peaks separated by e/C_{dot} were observed in the voltammograms, which were corresponding to the Coulomb staircases in the STS measurements. Cyclic voltammetry proved that E_c of Au NPs (1.64 nm diameters) exceeded ambient thermal fluctuation.[178]

Another novel observation in this report was that the 0D levels of the Au NPs affected the *I–V* characteristics. The observed d*I*/d*V* spectrum at 77 K included several peaks that could not be explained by the orthodox theory. These peaks indicated that the tunneling current increased because electrons were resonantly tunneling through the 0D levels.[54] The calculated mean energy level spacing ΔE was estimated to be 45 meV, which also surpassed the thermal broadening at 77 K ($3.5k_BT$ = 23 meV).

Au NPs with various ligand molecules have been investigated by STM: alkanethiols,[77,81–83,178,179,181,182] amino-type molecules,[84,183] dendrimers,[184] and polymers.[185,186] The ligand molecules works as linkers between the NPs and the substrate by physical or chemical interactions. Octanethiol–octanedithiol-mixed ligands were used to anchor the 1.5 nm-diameter NPs to a bare Au(111) surface.[181] The driving force in anchoring the NPs is attributed to the strong affinity of free thiols for Au atoms.[187] The force of the Au–S covalent bond is ≈180 kJ mol^{-1}, which is stronger than a hydrogen bond or van der Waals interaction.

978 | *Chem. Soc. Rev.*, 2015, **44**, 970–987

This journal is © The Royal Society of Chemistry 2015

The stability of this bond can be attributed to the observation of a stable Coulomb blockade at room temperature using octanethiol–octanedithiol-mixed ligands.[181]

Au NPs surrounded by citric acids are negatively charged; thus, they selectively adsorb onto a positively charged surface functionalized by amino-substituted thiols.[188,189] The Au NPs surrounded by amino-thiol can be anchored on a positively charged surface by carboxyl-substituted thiol as well.[84] Room-temperature Coulomb blockades have been reported using positively charged 1.8 nm-diameter Au NPs chemisorbed on a thiolactic acid/Au(111) surface (Fig. 11(c) and (d)).[84] Poly-(propylene imine) dendrimers (guest) can be immobilized on SAMs of heptathioether-functionalized β-cyclodextrin (host) through host–guest interactions.[184] The Au NPs protected by the dendrimer showed negative differential resistance peaks, attributed to the resonant tunneling of electrons through the molecular orbitals, in a room-temperature Coulomb staircase. Polyvinylpyrrolidone-protected Au NPs and Pd NPs on HOPG were used to control the charging energy of DBTJs.[185] The charging energy of the NPs was inversely proportional to the diameter of the NPs, which corresponds to the classical expression for the capacitance of a metal sphere in a dielectric medium ($4\pi\varepsilon R$, where ε is the dielectric constant of the medium and R is the diameter of the NPs).

Fig. 13 Observation of bandgap and 0D spectrum in semiconductor NPs by STS characterization. (a) Size evolution of dI/dV–V characteristics of single InAs NP at 4.2 K. The diameter of the NP ranges from 14 Å to 32 Å. The observed peaks are corresponding to resonant tunneling through the 0D energy levels of the NP.[196] Reprinted with permission from U. Banin, Y. Cao, D. Katz and O. Millo, *Nature*, 1999, **400**, 542–544. Copyright 1999 Macmillan Magazines Ltd. (b) dI/dV–V characteristics of single CdSe NP at 5 K. The diameter of the NP is 5 nm. The inset graph shows a good agreement of the experimental curves (black line) with theory (grey line).[201] Reproduced from ref. 201 with permission from the PCCP Owner Societies.
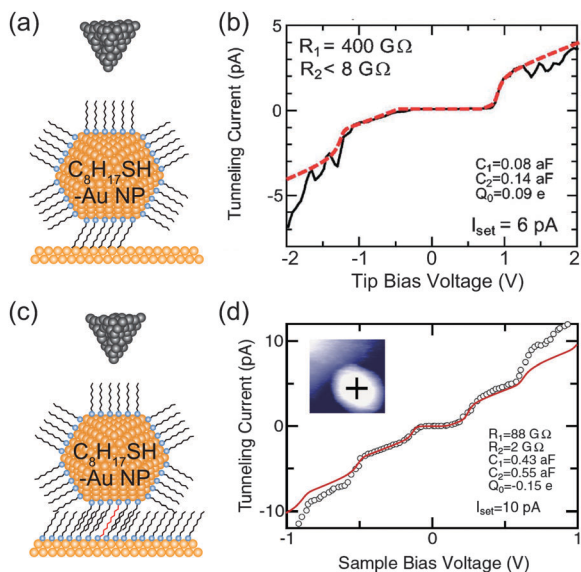

Fig. 12 Effects of physisorption and chemisorption on Coulomb staircases. (a) Schematic image of DBTJs consisting of PtIr-tip/octanethiol-protected Au nanoparticle/Au(111) structures. The NP is physisorbed on the Au(111). (b) Experimental and theoretical Coulomb staircases at 68 K on the physisorbed 2.4 nm-Au NP (solid and dashed lines, respectively).[81] Reprinted with permission from H. Zhang, Y. Yasutake, Y. Shichibu, T. Teranishi and Y. Majima, *Phys. Rev. B: Condens. Matter Mater. Phys.*, 2005, **72**, 205441. Copyright 2005 American Physical Society. (c) Schematic image of DBTJs consisting of PtIr-tip/octanethiol-protected Au nanoparticle/octanethiol, decanedithiol mixed SAMs/Au(111) structures. The NP is chemisorbed on the Au(111) *via* decanedithiol molecules. (d) Experimental and theoretical Coulomb staircases at 65 K on the chemisorbed 3.3 nm-Au NP (open circle and solid line, respectively).[83] Copyright (2010) The Japan Society of Applied Physics. The theoretical curves of (b) and (d) were calculated by the orthodox theory.
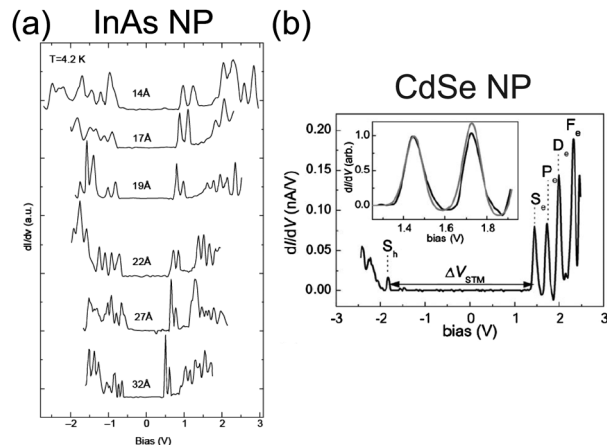
In our previous studies, we investigated physisorbed and chemisorbed Au NPs on Au(111) surfaces at low temperature. Fig. 12 shows two STS results on physisorbed and chemisorbed octanethiol-protected Au NPs. More clear and predictable Coulomb staircases are observed in the chemisorbed Au NPs anchored by decanedithiol. This result indicates that the chemisorption of NPs can be attributed to the stable electrical characteristics of NPs.[81,83]

Electrical characteristics of various synthesized NPs have been reported in addition to Au NPs: Ag,[85,190–193] Pt,[137] Co,[156,194] Pd,[168,169,185] Au–Ag alloy,[195] InAs,[85,196–198] CdS,[199] and CdSe.[78,200–202] Tuning the bandgap of InAs NPs linked to an Au surface by hexanedithiol molecules has been demonstrated between 0.9 and 1.9 eV by changing the diameter of the NPs between 1.0 and 3.5 nm (Fig. 13(a)).[196] The tunneling spectrum in the report indicated that an atomic-like Aufbau-principle filling of the s- and p-shells also occurred. The shell spectrum of CdSe and PbSe was quantitatively evaluated by low-temperature STS at 5 K (Fig. 13(b)).[201,202] Single-electron tunneling through the 0D levels observed by STS provides significant information about the 0D spectrum of NPs.

Reported single-electron effects of the synthesized NPs by STM are summarized in Table 2. The values of E_c are much larger than the thermal fluctuations at room temperature due to the small size of the NPs. It has been demonstrated that controlling the size of the synthesized NPs enables the control of E_c in SETs.[62] Therefore, synthesized NPs are good candidates for single Coulomb islands in SETs.

In this section, we described the history of the investigation of single-electron transport in single NPs by STM and STS. As the synthesis of NPs improved, several synthesized NPs have

This journal is © The Royal Society of Chemistry 2015

Chem. Soc. Rev., 2015, **44**, 970–987 | 979

Table 2 Reported single-electron effects on synthesized NPs by STS measurements. The core diameter (R) of the NPs, the experimental charging energy (E_c) of single NP and the observed temperature (T) of single-electron effects in the papers are summarized. Some of the E_c values are calculated by $E_c = e^2/2C_\Sigma$

Elements	Ligands	Sorption	R (nm)	E_c (meV)	T (K)	Ref.
Pt	Phenanthroline and O_2	Physisorption	1.68 ± 0.04	50	4.2	137
Au	$CH_3(CH_2)_5SH$	Physisorption	1.1–1.9	75–164	83	41, 178
Au	$(Ph_2PC_6H_4SO_3H)_{12}Cl_6$	Electrostatic interaction	<2	57	RT	76
Au	$CH_3(CH_2)_{11}SH$	Physisorption	1.7	75–167	RT	179
Au or Ag	Galvinol, $HS(CH_2)_6NH_2$, $CH_3(CH_2)_5SH$	Physisorption	2	30–148	RT	183
Au	$CH_3(CH_2)_6SH$	Physisorption	15 ± 2.1	10	4.2	77
			9.4 ± 1.5	19	4.2	
			4.6 ± 1.2	39	4.2	
			1.8 ± 0.6	>200	4.2	
Pt	Polyvinylpyrrolidone	Physisorption	2.5	100	RT	185
Au	Polyvinylpyrrolidone	Physisorption	1.7	220	RT	185
Ag	$CH_3(CH_2)_{11}SH$	Physisorption	3.5–7.7	300	RT	190
Co	$CH_3(CH_2)_{11}COOH$	Physisorption	5.5 ± 1.0	250	77	194
Ag	$CH_3(CH_2)_{11}SH$	Physisorption	4.3 ± 0.6	230–1000	RT	191
Au	$CH_3(CH_2)_{11}SH$	Physisorption	7 ± 0.4	76	5	194
Au	$CH_3(CH_2)_5SH$	Physisorption	2.1 ± 0.5	240–290	68	81
	$CH_3(CH_2)_7SH$	Physisorption	2.4 ± 0.5	140–360	68	81
Au	$CH_3(CH_2)_7SH$ and $HS(CH_2)_8SH$	Linked by $HS(CH_2)_8SH$	1.5	450	RT	181
Au	Poly(propyleneimine) dendrimer	Host–guest interaction	1.7 ± 0.9	67	RT	184
Au/Ag alloy	$CH_3(CH_2)_5SH$ and $HS(CH_2)_8SH$	Linked by $HS(CH_2)_8SH$	1–2	200	RT	195
Au	Triphenylphosphine	Linked by $HS(CH_2)_{10}SH$	<1	530	4.2	80
Au	$CH_3(CH_2)_7SH$	Linked by $HS(CH_2)_{10}SH$	3.3 ± 0.5	82	65	83
Au	Amino-type molecule	Electrostatic interaction	1.8 ± 0.2	200–450	RT	84
Au	Thiol-derivatized OPE	Linked by OPE derivative	2.1	570	100	87
InAs	Organic ligands	Linked by $HS(CH_2)_6SH$	1–4	110	4.2	196
CdS	N/A	Electrostatic interaction	2.1 ± 0.3	90–160	300	165
PbS	N/A	Electrostatic interaction	3.2 ± 0.4	80–120	300	166
CdSe	N/A	Physisorption	4.3 ± 0.4	60	4.2	78
CdSe	Hexylamine or pyridine	Linked by $HS(CH_2)_6SH$	3–5	>100 (0D spacing)	5	97
PbSe	Hexylamine or pyridine	Linked by $HS(CH_2)_6SH$	4	>100 (0D spacing)	5	97

RT: room temperature, N/A: not mentioned in the paper.

been characterized for applications in single-electron devices. Single-electron effects and electronic structures of a single NP can be revealed by STS measurements. The charging energy of a NP obtained by STS measurements is summarized in Table 2. STS is a powerful tool to explore candidates for Coulomb islands in single-electron transistors from the viewpoint of the charging energy.

4.2 Photon-emission from nanoparticles

Taking inelastic tunneling processes into consideration, it is expected that photons can be generated by inelastic electron tunneling between the STM tip and the substrate. Photon-emission in a single Ag NP has been explored with light-collection optics inside STM.[108,191,193,203–206] Ag NPs exhibit a surface plasmon resonance at a wavelength of around 400 nm.[203] The STM images and photon counts of an Ag NP were obtained simultaneously (Fig. 14(a)–(d)).[108,193,205] By using the spectrum analysis of the emitted photon energies, the in-plane and out-of-plane plasmon modes were excited in the SAMs of Ag NPs.[206] Photoluminescence switching was reproducibly observed in a single synthesized dodecanethiol-protected Ag NP on Au(111) at room temperature.[204] Detailed analysis of the photon-emission spectrum enables the observation of single-NP luminescence in several images at the tenth-nm scale. This technique allows us to observe the local excited luminescence of a nanomaterial.
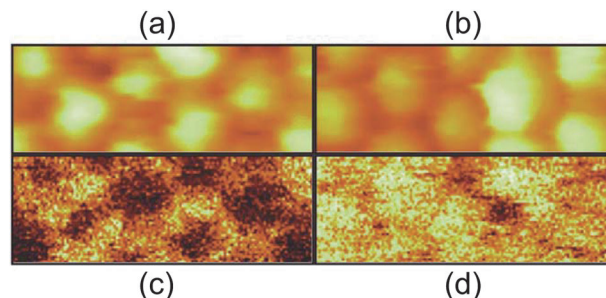

Fig. 14 Simultaneously recorded STM topography ((a), (b)) and photon mapping ((c), (d)) of thiol-coated Ag NPs. The scan area is 26×10 nm^2, sample bias voltage is 2.0 V in (a) and (c), 2.5 V in (b) and (d). The set-point current is 3.5 nA. White colour in the images represents a higher height and more photon emission.[108] Reproduced from F. Silly, F. Charra, Luminescence induced using a scanning-tunneling microscope as a nanophotonic probe, 2002, **3**, 493–500. Copyright 2002 Elsevier Masson SAS. All rights reserved.

4.3 Molecular vibrational modes on nanoparticles

Vibrational modes of molecules on synthesized NPs are important issues when we consider photon-emission from the NPs. The effects of a ligand's vibration have been observed on photon-emission from tunneling barriers, confirmed by STM and other optical spectroscopies. It is well known that Raman signals originating from molecular vibration can be enhanced due to a strong electric field on metallic NPs (Surface-enhanced
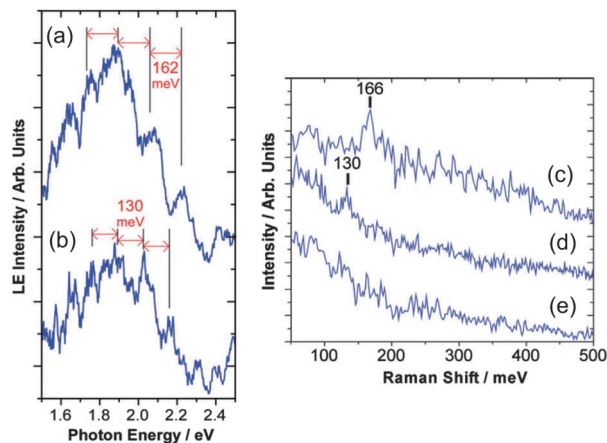
980 | *Chem. Soc. Rev.*, 2015, **44**, 970–987

This journal is © The Royal Society of Chemistry 2015

Fig. 15 Light emission spectrum of (a) a myristate-capped Ag NP/dode-canethiol/Au substrate and (b) a 2-methyl-1-propanethiolate Ag NP/dodecanethiol/Au substrate with STM observation. The spectrum has periodical peaks superimposed on a broad spectrum. The Raman spectrum of (c) a myristate-capped Ag NP/dodecanethiol/Au substrate, (d) a 2-methyl-1-propanethiolate Ag NP/dodecanethiol/Au substrate and (e) a dodecanethiol/Au substrate are shown. The Raman shifts of the NPs in (c) and (d) are corresponding to the periods of the peaks in (a) and (b), respectively. Thus, the peaks can be attributed to the molecular vibration of the capping molecules on the NPs. Adapted from ref. 211 with permission from the PCCP Owner Societies.

Fig. 16 (a) STM image of an individual Au$_{55}$ cluster protected by triphe-nylphosphine at 7 K. The light dots indicate phenyl rings of triphenylphos-phine. (b) Schematic illustration of the Au$_{55}$ cluster.[216] Reprinted with permission from G. Schmid and B. Corain, *Eur. J. Inorg. Chem.*, 2003, 3081–3098. Copyright 2003 Wiley-VCH. (c) STM image of octanethiol/mercaptopropionic acid mixed layer-protected Au NPs. The ligand shell shows phase separated ordered domains. Scale bar is 10 nm. (d) Schematic illustration of one single rippled NP. The yellow lobes represent octa-nethiols and the red lobes represent mercaptopropionic acids.[217] Reprinted with permission from A. M. Jackson, J. W. Myerson and F. Stellacci, *Nat. Mater.*, 2004, **3**, 330–336. Copyright 2004 Nature Publishing Group.

Raman scattering: SERS).[207–210] Raman spectroscopy and STM experiments were carried out on a myristate-capped Ag NP and a 2-methyl-1-propanethiolate Ag NP onto dodecanethiol/Au substrates, which shows that the vibration of ligand molecules affects the photon emission from the samples (Fig. 15).[211] High-resolution STM observation and Fourier transform infra-red spectroscopy found the relationship between homogeneity of a mixed monolayer (1-octanethiol and its fully deuterated analogues) and CH$_2$ stretching frequencies.[212] Tunneling current through single NPs can be modulated by inelastic electron tunneling due to molecular vibration on the NPs;[58] therefore, STS measurements are possible to detect the vibration of ligands and absorbed molecules on single NPs. In these two sections, we showed that STM and STS are useful tools in the fields of nanophotonics, the same as nanoelectronics.

4.4 Surface morphology of molecules on nanoparticles

STM imaging techniques can obtain fruitful information regarding the ligand molecules on NPs. Structural understanding of NPs has been obtained by transmission electron microscopy and X-ray crystallography.[213–215] Transmission electron microscopy is widely used to evaluate the size distribution and crystal structure of NPs. However, it is difficult to detect a thin ligand layer using the highly accelerated electron beam because most of the electrons penetrate the layer. X-ray diffraction gives information about a thin organic monolayer on a metal surface by the diffraction pattern. Conversely, STM can directly create an image of the ligand layer in real space, such as the morpho-logy and electron density distribution. Low-temperature STM has been used to visualize the phenyl rings of ligand molecules at 7 K under UHV conditions, which was correlated with a
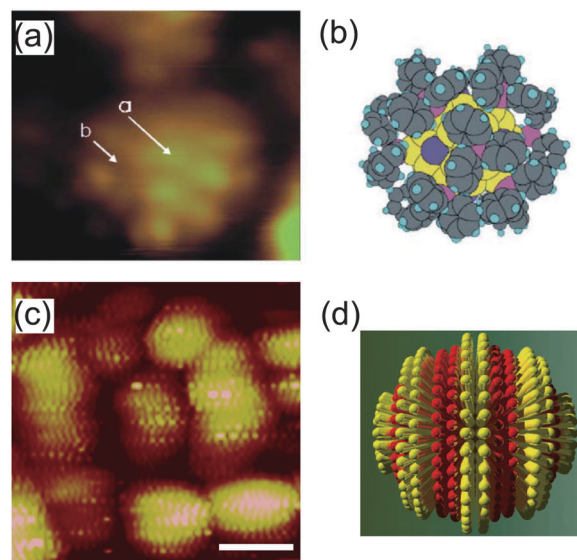
model (Fig. 16(a) and (b)).[39,216] High-resolution STM images of a mixed-ligand layer (*e.g.*, octanethiol and mercaptopropionic acid) on Au and Ag NPs have also been reported.[212,217–222] The observed images indicated that each ligand formed domains that were aligned to parallel ripples that spiraled around the NPs (Fig. 16(c) and (d)). The same group revealed that the mechanism for SAM formation on NPs is different from that on flat surfaces; the morphology is dependent on the diameter of NPs and the types of molecules.

The height of the NPs in the STM images also affords morphological information about the ligand molecules. The lateral width of the STM images is broader than the true width of the objects because of tip convolution effects.[223,224] In con-trast, the height and distance between the NPs are not affected by the convolution of the STM tip and the objects.[223] Therefore, it is more accurate to evaluate the diameter of NPs, including the ligands, from the height of the STM images. Ref. 49 showed that the height of the NPs in the image (2.2 nm) agreed well with the core diameter of the NPs (1.0 nm) and the height of the porphyrin molecules (0.6 nm), and hence proved the coordina-tion pattern of thiol-derivatized porphyrins to Au NPs (*e.g.*, six porphyrin faces surrounding each Au NP in a hexahedron).

By considering the set-point current dependence of a Coulomb staircase, the tunneling resistances of DBTJs can be estimated.[81,84,87] Resistances of alkanethiols,[81] a series of acid and base molecules,[84] and OPE[87] have been analyzed using the set-point current dependence. Zhang *et al.* estimated the
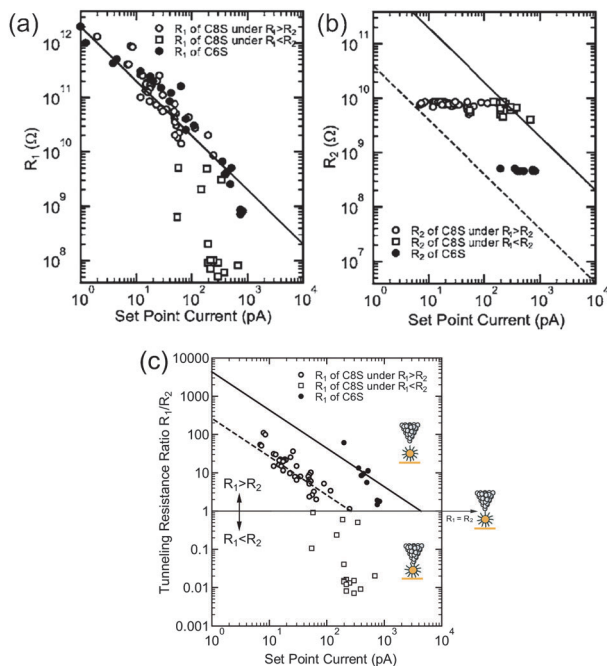
Fig. 17 Set-point current dependence of (a) tunneling resistance R_1, (b) tunneling resistance R_2, and (c) tunneling resistance ratio R_1/R_2 under the structure STM-tip/hexanethiol (octanethiol)-protected Au NP/Au(111). Open circles represent octanethiol protected Au NP in the region of $R_1 > R_2$, open squares represent octanethiol-protected Au NP in the region of $R_1 > R_2$, and closed circles represent hexanethiol-protected Au NP.[81] The dashed and solid lines show the relationship of the set-point current I_{set} and R_1/R_2, i.e., $I_{set}R_1/R_2 = -260$ pA ($V_{set}R_2 = -2$ V/7.6 GΩ) and $I_{set}R_1/R_2 = -4.3$ nA ($V_{set}R_2 = -2$ V/460 MΩ) for octanethiol and hexanethiol protected Au NPs, respectively. Reprinted with permission from H. Zhang, Y. Yasutake, Y. Shichibu, T. Teranishi and Y. Majima, *Phys. Rev. B: Condens. Matter Mater. Phys.*, 2005, **72**, 205441. Copyright 2005 American Physical Society.

resistance of hexanethiol and octanethiol on Au NPs as 460 MΩ and 7.6 GΩ, respectively (Fig. 17). It is noted that these tunneling resistances can be compared with those on reported solid-state single-electron transistors.[62,63] STS is also a powerful tool to explore candidates for Coulomb islands in single-electron transistors from the viewpoint of the tunneling resistance.

In this section, we showed that STM can provide information regarding the ligand molecules, such as the morphology, length, and tunneling resistance. Molecular-resolution STM reveals the geometrical order of ligand molecules on NPs. The length of ligand molecules can be estimated owing to the high sensitivity of the height information given by STM. The set-point current dependence of a Coulomb staircase provides the tunneling resistance of a ligand molecule on synthesized NPs.

4.5 Electrical-switching effects in single nanoparticles

Electrical-switching effects comprising functionalized NPs are interesting in possible applications of NPs.[31,225,226] For example, a photoirradiation-induced switching of nanoparticle monolayers was attributed to the reversible photoisomerization of the diarylethene molecules bridging the NPs.[225] A molecular floating-gate effect obtained by visible-light irradiation was observed in SETs with copper-phthalocyanine-doped Au NPs.[68] In principle, the NP

switching is due to the reversible properties of the ligands or linker molecules. STM has demonstrated many single-molecule switching effects in molecules such as OPE,[227,228] endohedral metallofullerenes,[8,15] and porphyrin and phthalocyanine derivatives.[21,95,97,98] Therefore, it is possible to observe the switching phenomena of a single functionalized NP by STM.

Blinking STM images of Au NPs tethered to thiol molecules have been reported.[87,229] These blinking events, which were reversible and stochastic, were observed in alkanedithiol and OPE molecules inserted into alkanethiol SAMs.[228,229] In this measurement, Au NPs were introduced to mark the blinking molecules. The blinking STM images were observed even after the attachment of Au NPs to the linker dithiol molecules; thus, the researchers concluded that the switching was caused by the thermally activated movement of the molecules tethered to the Au surface. The observed reversible switching was not attributed to breaking of the thiol–Au bond or a change in the free thiol group. There is also a report stating that the conductivity of Au NPs can be switched through redox effects of the linker molecule.[86] Because the decay length of an electron changes from 16 nm⁻¹ to 7 nm⁻¹ during redox, the conductivity of the Au NPs through Au(111) changed greatly.

A single Au NP protected by OPE ligands also showed stochastic blinking events (Fig. 18(a) and (b)).[87] The switching events had been observed several times during 80 min of continuous scanning. Decomposition or removal of the NPs
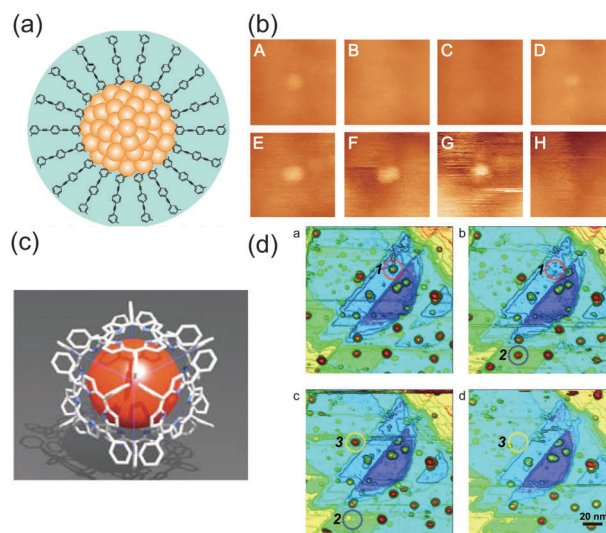

Fig. 18 (a) Schematic illustration of Au NPs protected by thiol-derivatized OPE. (b) Stochastic switching phenomena of the Au NP in successive STM scanning for 80 min.[87] The two solid lines are on the same Au NP and the height of the Au NP changes in the scans. Reprinted with permission from H. Koo, S. Kano, D. Tanaka, M. Sakamoto, T. Teranishi and Y. Majima, *Appl. Phys. Lett.*, 2012 **101**, 083115. Copyright 2012 American Institute of Physics. (c) Schematic illustration of Au NPs protected by thiol-derivatized porphyrin molecules. (d) Erase manipulation of the Au NPs by the STM tip during successive STM scanning. Applying 3 V between the STM tip and the substrate makes the NPs disappear.[49] Reprinted with permission from M. Sakamoto, D. Tanaka, H. Tsunoyama, T. Tsukuda, Y. Minagawa, Y. Majima and T. Teranishi, *J. Am. Chem. Soc.*, 2012 **134**, 816–819. Copyright 2012 American Chemical Society.

982 | *Chem. Soc. Rev.*, 2015, **44**, 970–987

This journal is © The Royal Society of Chemistry 2015

was not observed because the relative position of the NPs in the images did not change. This result shows the possible functionalization of variously sized NPs by surrounding ligands. In this case, stochastic switching due to single-molecular properties can be observed at scales larger than the molecules.

Sakamoto *et al.* demonstrated the erasure of Au NPs by STM at room temperature (Fig. 18(c) and (d)). The porphyrin-protected Au NPs were systematically removed by applying a voltage of 3.0 V to the Au NPs for 1 min. The quality of the STM images did not degrade even after erasing the NPs, which implies that the STM tip is kept clean during the erasing process. A possible mechanism for erasure may be the multistep reductive dissociation or heat decomposition of the NPs by inelastic tunneling currents. This erasure can be used as one-time write memory if we define the presence (absence) of NPs as 1 (0).

In this section, we summarized electrical-switching effects on NPs by using STM. The switching effects of NPs are attributed to the reversible physical properties of the surrounding molecules. Stochastic switching and one-time write switching have been reported as intriguing properties of single NPs. If we harness these switching phenomena, there appears a possibility for applying the solid-state memory device based on NPs.

5 Conclusions

STM and STS have become invaluable tools to characterize electrical and photonic properties of single synthesized NPs owing to the sub-nanometre scale topographies and measurements. Single electron effects of NPs, such as Coulomb blockades, have been demonstrated in detail, when combined with the theoretical calculation. The structural and electrical properties of ligand molecules on NPs have been also investigated. Photonic studies have been carried out on NPs by STM, which detects photons generated from molecular tunneling barriers. Stochastic blinking effects and one-write erasing behaviors of NPs are promising functions for the introduction of solid-state nanoscale memories based on synthesized NPs. Characterization methods for NPs by STM and STS reviewed here cover the significant interest for the NP functions towards the realization of solid-state nanodevices, especially for the diverse applications of single-electron transistors, nanoscale sensors or memories.

Acknowledgements

References

1 G. Binnig, H. Rohrer, Ch. Gerber and E. Weibel, *Phys. Rev. Lett.*, 1982, **49**, 61.
2 J. Tersoff and D. R. Hamann, *Phys. Rev. B: Condens. Matter Mater. Phys.*, 1985, **31**, 2.
3 G. Binnig and H. Rohrer, *IBM J. Res. Dev.*, 1986, **30**, 355.
4 N. D. Lang, *Phys. Rev. B: Condens. Matter Mater. Phys.*, 1986, **34**, 5947.
5 R. M. Feenstra, J. A. Stroscio and A. P. Fein, *Surf. Sci.*, 1987, **181**, 295.
6 G. Binnig, H. Rohrer, Ch. Gerber and E. Weibel, *Phys. Rev. Lett.*, 1983, **50**, 120.
7 M. Kuwabara, D. R. Clarke and D. A. Smith, *Appl. Phys. Lett.*, 1990, **56**, 2396–2398.
8 Y. Yasutake, Z. Shi, T. Okazaki, H. Shinohara and Y. Majima, *Nano Lett.*, 2005, **5**, 1057–1060.
9 P. A. Christensen, *Chem. Soc. Rev.*, 1992, **21**, 197–208.
10 H. Rohrer, *Surf. Sci.*, 1994, **299**, 956.
11 R. Wiesendanger, *Scanning Probe Microscopy and Spectroscopy: Methods and Application*, Cambridge University Press, Cambridge, 1994.
12 P. G. Collins, A. Zettl, H. Bando, A. Thess and R. E. Smalley, *Science*, 1997, **278**, 100–103.
13 L. C. Venema, J. W. G. Wildöer, J. W. Janssen, S. J. Tans, H. L. J. Temminck Tuinstra, L. P. Kouwenhoven and C. Dekker, *Science*, 1999, **283**, 52–55.
14 G. Li, A. Luican and E. Y. Andrei, *Phys. Rev. Lett.*, 2009, **102**, 176804.
15 M. Iwamoto, D. Ogawa, Y. Yasutake, Y. Azuma, H. Umemoto, K. Ohashi, N. Izumi, H. Shinohara and Y. Majima, *J. Phys. Chem. C*, 2010, **114**, 14704–14709.
16 L. A. Bumm, J. J. Arnold, T. D. Dunbar, D. L. Allara and P. S. Weiss, *J. Phys. Chem. B*, 1999, **103**, 8122.
17 R. E. Holmlin, R. Haag, M. L. Chabinyc, R. F. Ismagilov, A. E. Cohen, A. Terfort, M. A. Rampi and G. M. Whitesides, *J. Am. Chem. Soc.*, 2001, **123**, 5075–5085.
18 W. Wang, T. Lee and M. A. Reed, *Phys. Rev. B: Condens. Matter Mater. Phys.*, 2003, **68**, 035416.
19 X. Xiao, L. A. Nagahara, A. M. Rawlett and N. Tao, *J. Am. Chem. Soc.*, 2005, **127**, 9235–9240.
20 N. J. Tao, *Nat. Nanotechnol.*, 2006, **1**, 173–181.
21 S. Kano, Y. Yamada, K. Tanaka and Y. Majima, *Appl. Phys. Lett.*, 2012, **100**, 053101.
22 Y. Majima, D. Ogawa, M. Iwamoto, Y. Azuma, E. Tsurumaki and A. Osuka, *J. Am. Chem. Soc.*, 2013, **135**, 14159–14166.
23 W. P. Halperin, *Rev. Mod. Phys.*, 1986, **58**, 533–606.
24 A. P. Alivisatos, *Science*, 1996, **271**, 933–937.
25 C. N. R. Rao, G. U. Kulkarni, P. J. Thomas and P. P. Edwards, *Chem. Soc. Rev.*, 2000, **29**, 27–35.
26 T. Teranishi, *C. R. Chim.*, 2003, **6**, 979–987.
27 M.-C. Daniel and D. Astruc, *Chem. Rev.*, 2004, **104**, 293–346.
28 I. L. Medintz, H. T. Uyeda, E. R. Goldman and H. Mattoussi, *Nat. Mater.*, 2005, **4**, 435–446.
29 A. Z. Khosousi and A.-A. Dhirani, *Chem. Rev.*, 2008, **108**, 4072–4124.

30 D. V. Talapin, J.-S. Lee, M. V. Kovalenko and E. V. Shevchenko, *Chem. Rev.*, 2010, **110**, 389–458.

31 R. Klajn, J. F. Stoddart and B. A. Grzybowski, *Chem. Soc. Rev.*, 2010, **39**, 2203–2237.

32 M. Homberger and U. Simon, *Philos. Trans. R. Soc., A*, 2010, **368**, 1405–1453.

33 A. Verma and F. Stellacci, *Small*, 2010, **6**, 12–21.

34 F. A. Zwanenburg, A. S. Dzurak, A. Morello, M. Y. Simmons, L. C. L. Hollenberg, G. Klimeck, S. Rogge, S. N. Coppersmith and M. A. Eriksson, *Rev. Mod. Phys.*, 2013, **85**, 961–1019.

35 X. Cheng, S. B. Lowe, P. J. Reece and J. J. Gooding, *Chem. Soc. Rev.*, 2014, **43**, 2680–2700.

36 A. Comin and L. Manna, *Chem. Soc. Rev.*, 2014, **43**, 3957–3975.

37 S. M. Reimann and M. Manninen, *Rev. Mod. Phys.*, 2002, **74**, 1283–1342.

38 W. G. van der Wiel, S. De Franceschi, J. M. Elzerman, T. Fujisawa, S. Tarucha and L. P. Kouwenhoven, *Rev. Mod. Phys.*, 2003, **75**, 1–22.

39 G. Schmid, *Chem. Rev.*, 1992, **92**, 1709–1727.

40 M. Brust, M. Walker, D. Bethell, D. J. Schiffrin and R. Whyman, *J. Chem. Soc., Chem. Commun.*, 1994, 801.

41 S. Chen, R. S. Ingram, M. J. Hostetler, J. J. Pietron, R. W. Murray, T. G. Schaaff, J. T. Khoury, M. M. Alvarez and R. L. Whetten, *Science*, 1998, **280**, 2098–2101.

42 S. Chen, *J. Phys. Chem. B*, 2000, **104**, 663–667.

43 M. Brust and C. J. Kiely, *Colloids Surf., A*, 2002, **202**, 175–186.

44 G. H. Woehrle, M. G. Warner and J. E. Hutchison, *J. Phys. Chem. B*, 2002, **106**, 9979–9981.

45 T. Teranishi, S. Hasegawa, T. Shimizu and M. Miyake, *Adv. Mater.*, 2001, **13**, 1699–1701.

46 M. Kanehara, Y. Oumi, T. Sano and T. Teranishi, *J. Am. Chem. Soc.*, 2003, **125**, 8708–8709.

47 Y. Shichibu, Y. Negishi, T. Tsukuda and T. Teranishi, *J. Am. Chem. Soc.*, 2005, **127**, 13464–13465.

48 E. S. Shibu, M. A. Habeeb Muhammed, T. Tsukuda and T. Pradeep, *J. Am. Chem. Soc.*, 2008, **112**, 12168–12176.

49 M. Sakamoto, D. Tanaka, H. Tsunoyama, T. Tsukuda, Y. Minagawa, Y. Majima and T. Teranishi, *J. Am. Chem. Soc.*, 2012, **134**, 816–819.

50 M. Sakamoto, D. Tanaka and T. Teranishi, *Chem. Sci.*, 2013, **4**, 824.

51 M. L. Mastronardi, F. M. Flaig, D. Faulkner, E. J. Henderson, C. Kübel, U. Lemmer and G. A. Ozin, *Nano Lett.*, 2012, **12**, 337–342.

52 H. Sugimoto, M. Fujii, K. Imakita, S. Hayashi and K. Akamatsu, *J. Phys. Chem. C*, 2013, **117**, 11850–11857.

53 F. Kuemmeth, K. I. Bolotin, S.-F. Shi and D. C. Ralph, *Nano Lett.*, 2008, **8**, 4506–4512.

54 S. Kano, Y. Azuma, K. Maeda, D. Tanaka, M. Sakamoto, T. Teranishi, L. W. Smith, C. G. Smith and Y. Majima, *ACS Nano*, 2012, **6**, 9972.

55 L. M. Wheeler, N. R. Neale, T. Chen and U. R. Kortshagen, *Nat. Commun.*, 2013, **4**, 2197.

56 D. L. Klein, R. Roth, A. K. L. Lim, A. P. Alivisatos and P. L. McEuen, *Nature*, 1997, **389**, 699–701.

57 T. Sato, H. Ahmed, D. Brown and B. F. G. Johnson, *J. Appl. Phys.*, 1997, **82**, 696–701.

58 K. Luo, D.-H. Chae and Z. Yao, *Nanotechnology*, 2007, **18**, 465203.

59 V. Ray, R. Subramanian, P. Bhadrachalam, L.-C. Ma, C.-U. Kim and S. J. Koh, *Nat. Nanotechnol.*, 2008, **3**, 603–608.

60 Y. Azuma, Y. Yasutake, K. Kono, M. Kanehara, T. Teranishi and Y. Majima, *Jpn. J. Appl. Phys.*, 2010, **49**, 090206.

61 Y. Azuma, S. Suzuki, K. Maeda, N. Okabayashi, D. Tanaka, M. Sakamoto, T. Teranishi, M. R. Buitelaar, C. G. Smith and Y. Majima, *Appl. Phys. Lett.*, 2011, **99**, 073109.

62 N. Okabayashi, K. Maeda, T. Muraki, D. Tanaka, M. Sakamoto, T. Teranishi and Y. Majima, *Appl. Phys. Lett.*, 2012, **100**, 033101.

63 K. Maeda, N. Okabayashi, S. Kano, S. Takeshita, D. Tanaka, M. Sakamoto, T. Teranishi and Y. Majima, *ACS Nano*, 2012, **6**, 2798.

64 G. Hackenberger, S. Kano, Y. Azuma, S. Takeshita, D. Tanaka, M. Sakamoto, T. Teranishi, Y. Ohno, K. Maehashi, K. Matsumoto and Y. Majima, *Jpn. J. Appl. Phys.*, 2013, **52**, 110101.

65 S. Kano, Y. Azuma, D. Tanaka, M. Sakamoto, T. Teranishi, L. W. Smith, C. G. Smith and Y. Majima, *J. Appl. Phys.*, 2013, **114**, 223717.

66 Y. Noguchi, T. Terui, T. Katayama, M. M. Matsushita and T. Sugawara, *J. Appl. Phys.*, 2010, **108**, 094313.

67 M. Yamamoto, T. Terui, R. Ueda, K. Imazu, K. Tamada, T. Sakano, K. Matsuda, H. Ishii and Y. Noguchi, *Appl. Phys. Lett.*, 2012, **101**, 023103.

68 Y. Noguchi, M. Yamamoto, H. Ishii, R. Ueda, T. Terui, K. Imazu, K. Tamada, T. Sakano and K. Matsuda, *Jpn. J. Appl. Phys.*, 2013, **52**, 110102.

69 J. Liao, L. Bernard, M. Langer, C. Schönenberger and M. Calame, *Adv. Mater.*, 2006, **18**, 2444–2447.

70 Q. Sun, Y. A. Wang, L. S. Li, D. Y. Wang, T. Zhu, J. Xu, C. H. Yang and Y. F. Li, *Nat. Photonics*, 2007, **1**, 717–722.

71 C. Schönenberger, H. V. Houten and H. C. Donkersloot, *Europhys. Lett.*, 1992, **20**, 249.

72 D. Anselmetti, T. Richmond, A. Baratoff, G. Borer, M. Dreier, M. Bernasconi and H.-J. Güntherodt, *Europhys. Lett.*, 1994, **25**, 297–302.

73 M. Dorogi, J. Gomez, R. Osifchin, R. P. Andres and R. Reifenberger, *Phys. Rev. B: Condens. Matter Mater. Phys.*, 1995, **52**, 9071–9077.

74 R. P. Andres, T. Bein, M. Dorogi, S. Feng, J. I. Henderson, C. P. Kubiak, W. Mahoney, R. Osifchin and R. Reifenberger, *Science*, 1996, **272**, 1323–1325.

75 R. P. Andres, S. Datta, M. Dorogi, J. Gomez, J. I. Henderson, D. B. Janes, V. R. Kolagunta, C. P. Kubiak, W. Mahoney, R. F. Osifchin, R. Reifenberger, M. P. Smanta and W. Tian, *J. Vac. Sci. Technol., A*, 1996, **14**, 1178–1183.

76 L. F. Chi, M. Hartig, T. Drechsler, Th. Schwaach, C. Seidel, H. Fuchs and G. Schmid, *Appl. Phys. A: Mater. Sci. Process.*, 1998, **66**, S187–S190.

77 B. Wang, H. Wang, H. Li, C. Zeng, J. G. Hou and X. Xiao, *Phys. Rev. B: Condens. Matter Mater. Phys.*, 2000, **63**, 035403.

78 E. P. A. M. Bakkers, Z. Hens, A. Zunger, A. Franceschetti, L. P. Kouwenhoven, L. Gurevich and D. Vanmaekelbergh, *Nano Lett.*, 2001, **1**, 551–556.

79 T. Baron, P. Gentile, N. Magnea and P. Mur, *Appl. Phys. Lett.*, 2001, **79**, 1175–1177.

80 R. K. Smith, S. U. Nanayakkara, G. H. Woehrle, T. P. Pearl, M. M. Blake, J. E. Hutchison and P. S. Weiss, *J. Am. Chem. Soc.*, 2006, **128**, 9266–9267.

81 H. Zhang, Y. Yasutake, Y. Shichibu, T. Teranishi and Y. Majima, *Phys. Rev. B: Condens. Matter Mater. Phys.*, 2005, **72**, 205441.

82 Y. Majima, Y. Azuma and K. Nagano, *Appl. Phys. Lett.*, 2005, **87**, 163110.

83 X. Li, Y. Yasutake, K. Kono, M. Kanehara, T. Teranishi and Y. Majima, *Jpn. J. Appl. Phys.*, 2009, **48**, 04C180.

84 S. Kano, Y. Azuma, M. Kanehara, T. Teranishi and Y. Majima, *Appl. Phys. Express*, 2010, **3**, 105003.

85 D. Mocatta, G. Cohen, J. Schattner, O. Millo, E. Rabani and U. Banin, *Science*, 2011, **332**, 77.

86 D. I. Gittins, D. Bethell, D. J. Schiffrin and R. J. Nichols, *Nature*, 2000, **408**, 67–69.

87 H. Koo, S. Kano, D. Tanaka, M. Sakamoto, T. Teranishi and Y. Majima, *Appl. Phys. Lett.*, 2012, **101**, 083115.

88 C. Vericat, M. E. Vela, G. Benitez, P. Carro and R. C. Salvarezza, *Chem. Soc. Rev.*, 2010, **39**, 1805–1834.

89 N. Camillone, C. E. D. Chidsey, G.-y. Liu and G. Scoles, *J. Chem. Phys.*, 1993, **98**, 3503.

90 G. E. Poirier and M. J. Tarlov, *Langmuir*, 1994, **10**, 2853.

91 G. E. Poirier and E. D. Pylant, *Science*, 1996, **272**, 1145–1148.

92 When a bias voltage is applied between the STM tip and the metal electrode, it is considered that electric field is applied to the alkanethiol monolayer. So in a strict sense, the electric potential of the alkanethiol monolayer is different from that of the metal electrode. Even if coherent conduction is assumed, the single electron transmission probability is not as simple as eqn (1). Moreover, electron transport through nano-scale systems, such as molecular systems, is a highly non-equilibrium statistical problem. A theoretical model on this subject has not yet been established up to the present. In the case of incoherent conduction through molecular systems in particular, more sophisticated theoretical models are required in the future. However, discussion on this subject is beyond our review paper.

93 J. G. Simmons, *J. Appl. Phys.*, 1963, **34**, 1793–1803.

94 M. F. Crommie, C. P. Lutz and D. M. Eigler, *Science*, 1993, **262**, 218–220.

95 F. Moresco, G. Meyer, K.-H. Rieder, H. Tang, A. Gourdon and C. Joachim, *Phys. Rev. Lett.*, 2001, **86**, 672.

96 J. Repp, G. Meyer, F. E. Olsson and M. Persson, *Science*, 2004, **305**, 493–495.

97 P. Liljeroth, J. Repp and G. Meyer, *Science*, 2007, **317**, 1203–1206.

98 S. W. Wu, N. Ogawa, G. V. Nazin and W. Ho, *J. Phys. Chem. C*, 2008, **112**, 5141–5244.

99 B. Xu and N. J. Tao, *Science*, 2003, **301**, 1221–1223.

100 B. Xu, P. Zhang and N. Tao, *Nano Lett.*, 2004, **4**, 1105–1108.

101 M. Kiguchi, S. Miura, K. Hara, M. Sawamura and K. Murakoshi, *Appl. Phys. Lett.*, 2006, **89**, 213104.

102 R. J. Hamers, R. M. Tromp and J. E. Demuth, *Phys. Rev. Lett.*, 1986, **56**, 1972–1975.

103 B. C. Stipe, M. A. Rezaei and W. Ho, *Science*, 1998, **280**, 1732–1735.

104 A. J. Heinrich, C. P. Lutz, J. A. Gupta and D. M. Eigler, *Science*, 2002, **298**, 1381–1387.

105 N. Okabayashi, Y. Konda and T. Komeda, *Phys. Rev. Lett.*, 2008, **100**, 217801.

106 J. K. Gimzewski, J. K. Sass, R. R> Schlitter and J. Schott, *Europhys. Lett.*, 1989, **8**, 435–440.

107 M. M. J. Bischoff, M. C. M. M. van der Wielen and H. van Kempen, *Surf. Sci.*, 1998, **400**, 127–133.

108 F. Silly and F. Charra, *C. R. Phys.*, 2002, **3**, 493–500.

109 H. Song, Y. Kim, Y. H. Jang, H. Jeong, M. A. Reed and T. Lee, *Nature*, 2009, **462**, 1039–1043.

110 A. Mangin, A. Anthore, M. L. Della Rocca, E. Boulat and P. Lafarge, *Phys. Rev. B: Condens. Matter Mater. Phys.*, 2009, **80**, 235432.

111 Y. Naitoh, S. Takeshita, D. Ishida, E. Ohmura, K. Kobayashi, H. Yamada and Y. Majima, *Appl. Phys. Express*, 2012, **5**, 085201.

112 K. K. Likharev, *Proc. IEEE*, 1999, **87**, 606.

113 Z. A. K. Durrani, *Single-Electron Devices and Circuits in Silicon; Imperial College*, London, 2009, ch. 2.

114 A. E. Hanna and M. Tinkham, *Phys. Rev. B: Condens. Matter Mater. Phys.*, 1991, **44**, 5919–5922.

115 M. A. Kastner, *Rev. Mod. Phys.*, 1992, **64**, 849–858.

116 K. Yano, T. Ishii, T. Hashimoto, T. Kobayashi, F. Murai and K. Seki, *IEEE Trans. Electron Devices*, 1994, **41**, 1628–1638.

117 J. P. Pekola, O.-P. Saira, V. F. Maisi, A. Kemppinen, M. Möttïen, Y. A. Pashkin and D. V. Averin, *Rev. Mod. Phys.*, 2013, **85**, 1421–1472.

118 L. Zhuang, L. Guo and S. Y. Chou, *Appl. Phys. Lett.*, 1998, **72**, 1205.

119 B. H. Choi, S. W. Hwang, L. G. Kim, H. C. Shin, Y. Kim and E. K. Kim, *Appl. Phys. Lett.*, 1998, **73**, 3129.

120 S. J. Shin, C. S. Jung, B. J. Park, T. K. Yoon, J. J. Lee, S. J. Kim, J. B. Choi, Y. Takahashi and D. G. Hasko, *Appl. Phys. Lett.*, 2010, **97**, 103101.

121 S. Lee, Y. Lee, E. B. Song and T. Hiramoto, *Nano Lett.*, 2014, **14**, 71–77.

122 H. W. Ch. Postma, T. Teepen, Z. Yao, M. Grifoni and C. Dekker, *Science*, 2001, **293**, 76–79.

123 M. Maeda, S. Iwasaki, T. Kamimura, K. Murata and K. Matsumoto, *Jpn. J. Appl. Phys.*, 2008, **47**, 5724.

124 Y. Oyama, Y. Majima and M. Iwamoto, *J. Appl. Phys.*, 1999, **86**, 7087.

125 Y. Azuma, M. Kanehara, T. Teranishi and Y. Majima, *Phys. Rev. Lett.*, 2006, **96**, 016108.

126 N. W. Ashcroft and N. D. Mermin, *Solid State Physics*, Saunder College Publishing, Philadelphia, PA, 1976.

127 M. Fujii, O. Mamezaki, S. Hayashi and K. Yamamoto, *J. Appl. Phys.*, 1998, **83**, 1507–1512.

128 Z. A. K. Durrani and M. A. Rafiq, *Microelectron. Eng.*, 2009, **86**, 456–466.

129 D. V. Averin, A. N. Korotkov and K. K. Likharev, *Phys. Rev. B: Condens. Matter Mater. Phys.*, 1991, **44**, 6199.

This journal is © The Royal Society of Chemistry 2015

Chem. Soc. Rev., 2015, **44**, 970–987 | 985

130 C. W. J. Beenakker, *Phys. Rev. B: Condens. Matter Mater. Phys.*, 1991, **44**, 1646–1656.

131 M. Pierre, R. Wacquez, X. Jehl, M. Ssanquer, M. Vinet and O. Cueto, *Nat. Nanotechnol.*, 2009, **5**, 133–137.

132 M. Fuechsle, S. Mahapatra, F. A. Zwanenburg, M. Friesen, M. A. Eriksson and M. Y. Simmons, *Nat. Nanotechnol.*, 2010, **5**, 502–506.

133 M. Fuechsle, J. A. Miwa, S. Mahapatra, H. Ryu, S. Lee, O. Warschkow, L. C. L. Hollenberg, G. Klimech and M. Y. Simmons, *Nat. Nanotechnol.*, 2012, **7**, 242–246.

134 S. Chen and R. W. Murray, *Langmuir*, 1999, **15**, 682–689.

135 S. Chen, *Langmuir*, 1999, **15**, 7551–7557.

136 F. Deng, Y. Yang, S. Hwang, Y.-S. Shon and S. Chen, *Anal. Chem.*, 2004, **76**, 6102–6107.

137 J. G. A. Dubois, J. W. Gerritssen, S. E. Shafranjuk, E. J. G. Boon, G. Schmid and H. van Kempen, *Europhys. Lett.*, 1996, **33**, 279–284.

138 H. Kitazawa, K. Albrecht and K. Yamamoto, *Chem. Lett.*, 2012, **41**, 828–830.

139 C. B. Murray, D. J. Norris and M. G. Bawendi, *J. Am. Chem. Soc.*, 1993, **115**, 8706–8715.

140 C. B. Murray, C. R. Kagan and M. G. Bawendi, *Science*, 1995, **270**, 1335–1338.

141 A. A. Guzelian, U. Banin, A. V. Kadavanich, X. Peng and A. P. Alivisatos, *Appl. Phys. Lett.*, 1996, **69**, 1432.

142 O. I. Micic, J. R. Sprague, C. J. Curtis, K. M. Jones, J. L. Machol, A. J. Nozik, H. Giessen, B. Fluegel, G. Mohs and N. Peyghambarian, *J. Phys. Chem.*, 1995, **99**, 7754–7759.

143 T. Teranishi and M. Miyake, *Chem. Mater.*, 1998, **10**, 594–600.

144 N. Zheng, J. Fan and G. D. Stucky, *J. Am. Chem. Soc.*, 2006, **128**, 6550–6551.

145 D. J. Fuchs and P. S. Weiss, *Nanotechnology*, 2010, **18**, 044021.

146 S. Hattori, S. Kano, Y. Azuma and Y. Majima, *J. Phys. Chem. C*, 2010, **114**, 8120–8125.

147 S. Hattori, S. Kano, Y. Azuma, D. Tanaka, M. Sakamoto, T. Teranishi and Y. Majima, *Nanotechnology*, 2012, **23**, 185704.

148 L. Kasprzak, R. Laibowitz, S. Head and M. Ohring, *Thin Solid Films*, 1974, **22**, 189–196.

149 I. Giaever and H. R. Zeller, *Phys. Rev. Lett.*, 1968, **20**, 1504.

150 J. Lambe and R. C. Jaklevic, *Phys. Rev. Lett.*, 1969, **22**, 1371–1375.

151 J. B. Barner and S. T. Ruggiero, *Phys. Rev. Lett.*, 1987, **57**, 807–810.

152 P. J. M. van Bentum, R. T. M. Smokers and H. van Kempen, *Phys. Rev. Lett.*, 1988, **60**, 2543–2546.

153 H. van Kempen, P. J. M. van Bentum and R. T. M. Smokers, *Phys. Scr., T*, 1992, **42**, 153–158.

154 E. Bar-Sadeh, Y. Goldstein, C. Zhang, H. Deng, B. Abeles and O. Millo, *Phys. Rev. B: Condens. Matter Mater. Phys.*, 1994, **50**, 8961–8964.

155 L. Wang, M. E. Taylor and M. E. Welland, *Surf. Sci.*, 1995, **322**, 325–336.

156 K. Schouteden, A. Lando, E. Janssens, C. V. Haesendonck and P. Lievens, *New J. Phys.*, 2008, **10**, 083005.

157 R. Wilkins, E. Ben-Jacob and R. C. Jaklevic, *Phys. Rev. Lett.*, 1989, **63**, 801–804.

158 M. Amman, R. Wilkins, E. Ben-Jacob, P. D. Maker and R. C. Jaklevic, *Phys. Rev. B: Condens. Matter Mater. Phys.*, 1991, **43**, 1146–1149.

159 J.-C. Wan, K. A. McGreer, N. Anand, E. Nowak and A. M. Goldman, *Phys. Rev. B: Condens. Matter Mater. Phys.*, 1990, **42**, 5604–5609.

160 A. Bettac, L. Köller, V. Rank and K. H. Meiwes-Broer, *Surf. Sci.*, 1998, **402–404**, 475–479.

161 H. N. Aier, V. Vijayakrishnan, G. N. Subbanna and C. N. R. Rao, *Surf. Sci.*, 1994, **313**, 392–398.

162 C. P. Vinod, G. U. Kulkarni and C. N. R. Rao, *Chem. Phys. Lett.*, 1998, **289**, 329–333.

163 N. Camillone III, T. Y. B. Leung, P. Schwartz, P. Eisenberger and G. Scoles, *Langmuir*, 1996, **12**, 2737.

164 M. P. Samanta, W. Tian, S. Datta, J. I. Henderson and C. P. Kubiak, *Phys. Rev. B: Condens. Matter Mater. Phys.*, 1996, **53**, 7626.

165 P. Jiang, Z. F. Liu and S. M. Cai, *Appl. Phys. Lett.*, 1999, **75**, 3023–3025.

166 P. Jiang, Z. F. Liu and S. M. Cai, *J. Appl. Phys.*, 2001, **90**, 2039–2041.

167 R. Breitwieser, P. Campiglio, C. Chacon, V. Repain, R. Nemausat, Y. Girard, J. Lagoute and S. Rousset, *Surf. Sci.*, 2012, **606**, 542–548.

168 N. Oncel, A.-S. Hallback, H. J. W. Zandvliet, E. A. Speets, B. J. Ravoo, D. N. Reinhoudt and B. Poelsema, *J. Chem. Phys.*, 2005, **123**, 044703.

169 E. A. Speets, B. Dordi, B. J. Ravoo, N. Oncel, A.-S. Hallbäck, H. J. W. Zandvliet, B. Poelsema, G. Rijnders, D. H. A. Blank and D. N. Reinhoudt, *Small*, 2005, **1**, 395–398.

170 K. Schouteden, N. Vandamme, E. Janssen, P. Lievens and C. V. Haesendonck, *Surf. Sci.*, 2008, **602**, 552–558.

171 T. Ohgi, H.-Y. Sheng, Z.-C. Dong and H. Nejoh, *Surf. Sci.*, 1999, **442**, 277–282.

172 T. Ohgi, H.-Y. Sheng, Z.-C. Dong, H. Nejoh and D. Fujita, *Appl. Phys. Lett.*, 2001, **79**, 2453.

173 T. Ohgi and D. Fujita, *Phys. Rev. B: Condens. Matter Mater. Phys.*, 2002, **66**, 115410.

174 T. Ohgi and D. Fujita, *Surf. Sci.*, 2003, **532–535**, 294–299.

175 T. Ohgi, Y. Sakotsubo, Y. Ootuka and D. Fujita, *Appl. Phys. Lett.*, 2004, **84**, 604–606.

176 Y. Sakotsubo, T. Ohgi, D. Fujita and Y. Ootuka, *Physica E*, 2005, **29**, 601–605.

177 H. van Kempen, J. G. A. Dubois, J. W. Gerritssen and G. Schmid, *Physica B*, 1995, **204**, 51–56.

178 R. S. Ingram, M. J. Hostetler, R. W. Murray, T. G. Schaaff, J. T. Khoury, R. L. Whetten, T. P. Bigioni, D. K. Guthrie and P. N. First, *J. Am. Chem. Soc.*, 1997, **119**, 9279–9280.

179 T. P. Bigioni, L. E. Harrell, W. G. Cullen, D. K. Guthrie, R. L. Whetten and P. N. First, *Eur. Phys. J. D*, 1999, **6**, 355–364.

180 F.-R. F. Fan and A. J. Bard, *Science*, 1997, **277**, 1791–1793.

181 G. Yang, L. Tan, Y. Yang, S. Chen and G.-Y. Liu, *Surf. Sci.*, 2005, **589**, 129–138.

182 P. Yang, I. Arfaoui, T. Cren, N. Goubet and M.-P. Pileni, *Phys. Rev. B: Condens. Matter Mater. Phys.*, 2012, **86**, 075409.

986 | *Chem. Soc. Rev.*, 2015, **44**, 970–987

This journal is © The Royal Society of Chemistry 2015

183 W. P. McConnell, J. P. Novak, L. C. Brousseau III, R. R. Fuierer, R. C. Tenent and D. L. Feldheim, *J. Phys. Chem. B*, 2000, **104**, 8925–8930.

184 C. A. Nijhuis, N. Oncel, J. Huskens, H. J. W. Zandvliet, B. J. Ravoo, B. Poelsema and D. N. Reinhoudt, *Small*, 2006, **2**, 1422–1426.

185 P. John Thomas, G. U. Kulkarni and C. N. R. Rao, *Chem. Phys. Lett.*, 2000, **321**, 163–168.

186 A. Naitabdi, L. K. Ono and B. Roldan Cuenya, *Appl. Phys. Lett.*, 2006, **89**, 043101.

187 L. H. Dubois and R. G. Nuzzo, *Annu. Rev. Phys. Chem.*, 1992, **43**, 437–463.

188 L. Jiang, A. Eitan, L. S. Schadler, P. M. Ajayan, R. W. Siegel, N. Grober, M. Mayne, M. Reyes-Reyes, H. Terrones and M. Terrones, *Nano Lett.*, 2003, **3**, 275.

189 R. Zanella, E. V. Basiuk, P. Santiago, V. A. Basiuk, E. Mireles, I. Puente-Lee and J. M. Saniger, *J. Phys. Chem. B*, 2005, **109**, 16290–16295.

190 R. C. Doty, H. Yu, C. K. Shih and B. A. Korgel, *J. Phys. Chem. B*, 2001, **105**, 8291–8296.

191 A. Taleb, F. Silly, A. O. Gusev, F. Charra and M.-P. Pileni, *Adv. Mater.*, 2000, **12**, 633–637.

192 A. O. Gusev, A. Taleb, F. Silly, F. Charra and M.-P. Pileni, *Adv. Mater.*, 2000, **12**, 1583–1588.

193 N. Nilius, H.-M. Benia, C. Salzemann, G. Rupprechter, H.-J. Freund, A. Brioude and M.-P. Pileni, *Adv. Mater.*, 2000, **12**, 1583–1588.

194 C. Petit, T. Cren, D. Roditchev, W. Sacks, J. Klein and M.-P. Pileni, *Adv. Mater.*, 1998, **11**, 1198–1202.

195 S. Devarajan and S. Sampath, *Chem. Phys. Lett.*, 2006, **424**, 105–110.

196 U. Banin, Y. Cao, D. Katz and O. Millo, *Nature*, 1999, **400**, 542–544.

197 O. Millo, D. Katz, Y. Cao and U. Banin, *Phys. Rev. B: Condens. Matter Mater. Phys.*, 2000, **61**, 16773–16777.

198 L. I. Halaoui, R. L. Wells and L. A. Coury Jr, *Chem. Mater.*, 2000, **12**, 1205–1216.

199 S. Ogawa, F.-R. F. Fan and A. J. Bard, *J. Phys. Chem.*, 1995, **99**, 11182–11189.

200 B. Alperson, I. Rubinstein, G. Hodes, D. Porath and O. Millo, *Appl. Phys. Lett.*, 1999, **75**, 1751.

201 P. Liljeroth, L. Jdira, K. Overgaag, B. Grandidier, S. Speller and D. Vanmaekelbergh, *Phys. Chem. Chem. Phys.*, 2006, **8**, 3845–3850.

202 K. Overgaag, P. Liljeroth, B. Grandidier and D. Vanmaekelbergh, *ACS Nano*, 2008, **2**, 600–606.

203 K. Ertel, U. Kohl, J. Lehmann, M. Merschdorf, W. Pfeiffer, A. Thon, S. Voll and G. Gerber, *Appl. Phys. B: Lasers Opt.*, 1999, **68**, 439–445.

204 F. Silly, A. O. Gusev, F. Charra, A. Taleb and M.-P. Pileni, *Appl. Phys. Lett.*, 2001, **79**, 4013–4015.

205 F. Silly, A. O. Gusev, A. Taleb, M.-P. Pileni and F. Charra, *Mater. Sci. Eng., C*, 2002, **19**, 193–195.

206 N. Nilius, H.-M. Benia, C. Salzemann, G. Rupprechter, H.-HJ. Freund, A. Brioude and M.-P. Pileni, *Chem. Phys. Lett.*, 2005, **413**, 10–15.

207 B. Pettinger, G. Picardi, R. Schuster and G. Ertl, *Single Mol.*, 2002, **5**, 285–294.

208 D. R. Ward, N. J. Halas, J. W. Ciszek, J. M. Tour, Y. Wu, P. Nordlander and D. Natelson, *Nano Lett.*, 2008, **8**, 919–924.

209 F. Rossel, M. Pivetta and W.-D. Schneider, *Surf. Sci. Rep.*, 2010, **65**, 129–144.

210 J. F. Li, Y. F. Huang, Y. Ding, Z. L. Yang, S. B. Li, X. S. Zhou, F. R. Fan, W. Zhang, Z. Y. Zhou, D. Y. Wu, B. Ren, Z. L. Wang and Z. Q. Tian, *Nature*, 2010, **464**, 392–395.

211 S. Katano, K. Toma, M. Toma, K. Tamada and Y. Uehara, *Phys. Chem. Chem. Phys.*, 2010, **12**, 14749–14753.

212 A. Centrone, Y. Hu, A. M. Jackson, G. Zerbi and F. Stellacci, *Small*, 2007, **3**, 814–817.

213 P. D. Jadzinsky, G. Calero, C. J. Ackerson, D. A. Bushnell and R. D. Kornberg, *Science*, 2007, **318**, 430.

214 M. Walter, J. Akola, O. Lopez-Acevedo, P. D. Jadzinsky, G. Calero, C. J. Ackerson, R. L. Whetten, H. Grönbech and H. Häkkinen, *Proc. Natl. Acad. Sci. U. S. A.*, 2008, **105**, 9157–9162.

215 H. Häkkinen, *Nat. Chem.*, 2012, **4**, 443–455.

216 G. Schmid and B. Corain, *Eur. J. Inorg. Chem.*, 2003, 3081–3098.

217 A. M. Jackson, J. W. Myerson and F. Stellacci, *Nat. Mater.*, 2004, **3**, 330–336.

218 A. M. Jackson, Y. Hu, P. J. Silva and F. Stellacci, *J. Am. Chem. Soc.*, 2006, **128**, 11135–11149.

219 C. Singh, P. K. Ghorai, M. A. Horsch, A. M. Jackson, R. G. Larson, F. Stellacci and S. C. Glotzer, *Phys. Rev. Lett.*, 2007, **99**, 226106.

220 X. Liu, M. Yu, H. Kim, M. Mameli and F. Stellacci, *Nat. Commun.*, 2012, **3**, 1182.

221 Q. K. Ong, J. Riguera, P. J. Silva, M. Moglianetti, K. Harkness, M. Longobardi, K. S. Mali, C. Renner, S. D. Feyter and F. Stellacci, *ACS Nano*, 2013, **7**, 8529–8539.

222 F. Biscarini, Q. K. Ong, C. Albonetti, F. Liscio, M. Longobardi, K. S. Mali, A. Ciesielski, J. Reguera, C. Renner, S. D. Feyter, P. Samori and F. Stellacci, *Langmuir*, 2013, **29**, 13723–13734.

223 J. Barbet, A. Garvin, J. Thimonier, J.-P. Chauvin and J. Rocca-Serra, *Ultramicroscopy*, 1993, **50**, 355–363.

224 K. I. Schiffmann, M. Fryda, G. Goerigk, R. Lauer and P. Hinze, *Ultramicroscopy*, 1996, **66**, 183–192.

225 S. J. van der Molen and P. Liljeroth, *J. Phys.: Condens. Matter*, 2010, **22**, 133001.

226 S. J. van der Molen, J. H. Liao, T. Kudernac, J. S. Agustsson, L. Bernard, M. Calame, B. J. van Wees, B. L. Feringa and C. Schönenberger, *Nano Lett.*, 2009, **9**, 76–80.

227 Z. J. Donhauser, B. A. Mantooth, K. F. Kelly, L. A. Bumm, J. D. Monnell, J. J. Stapleton, D. W. Price Jr, A. M. Rawlett, D. L. Allara, J. M. Tour and P. S. Weiss, *Science*, 2001, **292**, 2303.

228 K.-H. Jung, E. Hase, Y. Yasutake, H.-K. Shin, Y.-S. Kwon and Y. Majima, *Jpn. J. Appl. Phys.*, 2006, **45**, L840.

229 G. K. Ramachandran, T. J. Hopson, A. M. Rawlett, L. A. Nagahara, A. Primak and S. M. Lindsay, *Science*, 2003, **300**, 1413–1415.

This journal is © The Royal Society of Chemistry 2015

Chem. Soc. Rev., 2015, **44**, 970–987 | 987